Time-Optimal Control for High-Order Chain-of-Integrators Systems with Full State Constraints and Arbitrary Terminal States

Yunan Wang, Chuxiong Hu, *Senior Member, IEEE,* Zeyang Li, Shize Lin, Suqin He, and Yu Zhu, *Member, IEEE*

***Abstract*—Time-optimal control for high-order chain-of-integrators systems with full state constraints and arbitrarily given terminal states remains a challenging problem in the optimal control theory domain, yet to be resolved. To enhance further comprehension of the problem, this paper establishes a novel notation system and theoretical framework, providing the switching manifold for high-order problems in the form of switching laws. Through deriving properties of switching laws regarding signs and dimension, this paper proposes a definite condition for time-optimal control. Guided by the developed theory, a trajectory planning method named the manifold-intercept method (MIM) is developed. The proposed MIM can plan time-optimal jerk-limited trajectories with full state constraints, and can also plan near-optimal non-chattering higher-order trajectories with negligible extra motion time compared to optimal profiles. Numerical results indicate that the proposed MIM outperforms all baselines in computational time, computational accuracy, and trajectory quality by a large gap.**

***Index Terms*—Optimal control, linear systems, variational methods, switched systems, trajectory planning.**

I. Introduction

HIGH-ORDER chain-of-integrators systems have been universally utilized in computer numerical control (CNC) machining [1], [2], robotic motion control [3], [4], [5], semiconductor device fabrication [6], [7], and autonomous driving [8]. Trajectory planning has a significant influence on motion efficiency and accuracy in those scenarios [9], [10]. However, time-optimal control for high-order chain-of-integrators systems with full state constraints and arbitrary terminal states remains a challenging and significant open problem in the optimal control theory domain, yet to be fully resolved.

The time-optimal control problem for chain-of-integrators requires planning a trajectory with minimum motion time from a given initial state vector to a terminal state vector, where the system state vector is composed of components such as position, velocity, acceleration, and so forth. State constraints require that all system state components are limited by given upper bounds, while the initial states and the terminal states are specified arbitrarily. A suboptimal fifth order trajectory planned by the proposed Algorithm 1 is shown in Fig. 1. The input control, i.e., crackle, and the system states, i.e., position, velocity, acceleration, jerk, and snap, are bounded by the given constraints. The control is always at its maximum, minimum, or zero value along the planned trajectory, satisfying the Bang-Singular-Bang control law [11].

Corresponding author: Chuxiong Hu (e-mail: cxhu@tsinghua.edu.cn). The authors are all with the Department of Mechanical Engineering, Tsinghua University, Beijing 100084, China.

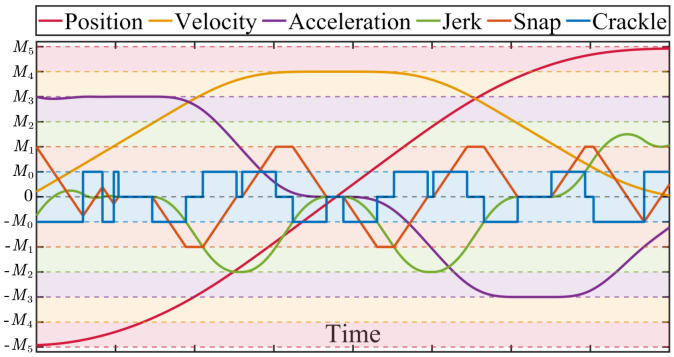

Fig. 1. A fifth order trajectory planned by the proposed method. M_5, M_4, M_3, M_2, M_1, and M_0 are the upper bounds of position, velocity, acceleration, jerk, snap, and crackle, respectively. The trajectory can be represented as $\underline{0}\overline{0}\,(\overline{3},2)\,\bar{0}\underline{0}\overline{0}3\underline{0}1\bar{0}\underline{2}0\overline{1}\underline{0}\bar{4}\underline{0}1\bar{0}\underline{2}0\overline{1}\underline{0}3\underline{0}1\underline{0}\overline{0}$ in Section III.

In optimal control, numerous research has been conducted on time-optimal control for chain-of-integrators. The problem with only input saturation has been fully solved based on Pontryagin's maximum principle (PMP) [12], where theorems on the Bang-Bang control [13] and the analytic expression of the optimal control [14] are well-known. Marchand et al. [15] proposed a discrete-time control law based on the above problem. However, the time-optimal problem with input saturation and full state constraints remains unsolved, especially when the initial and terminal states are arbitrarily given, i.e., the terminal states are allowed to be non-zero. The 2nd order problem is trivial [16], but 3rd or higher-order problems have not been solved well. Haschke et al. [17] proposed an online time-optimal jerk-limited trajectory planning method without position constraints. Kröger [18] developed the Reflexxes type IV motion library, solving the third order problem without given terminal acceleration and position constraints. Berscheid and Kröger [19] fully considered third order chain-of-integrators with arbitrary terminal states and no position constraints, resulting in a widely-used jerk-limited trajectory planning package, i.e., Ruckig. Some approaches on continuous path following time-optimal trajectory planning are proposed in [20], with an order lower than 3. To the best of our knowledge, there has been no mature method available for planning 4th order optimal trajectories with full state constraints so far.

For higher-order problems, the control invariant set [21]

and the switching surface [22] are significant tools, which provide the nature of the time-optimal problem [23]. Mitchell et al. [24] calculated the invariant set based on level sets of solutions of a partial differential equation. Tahir et al. [25] employed a polyhedral approximation to characterize the invariant set. Doeser et al. [26] constructed the third order invariant sets for integrators. Yury [27] obtained the switching surface for the 3rd order problem in part. He et al. [11] provided the explicitly analytic expressions of the complete switching surfaces for the 3rd order problem with zero terminal states. However, the investigation of switching surfaces for 3rd order problems remains incomplete, while limited studies on switching manifold have been conducted for 4th order or higher-order problems. Specifically, the existence of chattering phenomena [28], i.e., the control switching for infinite times in a finite time period, still remains unknown in the investigated problem, let alone optimal control.

Since higher-order problems are lack of theoretical results, scholars either discretize the continuous-time problem and solve the discrete problem using numerical optimization, or plan feasible-but-not-optimal trajectories in engineering. Direct methods have been widely applied in numerical optimal control problems, and some optimization solvers have been built, such as CasADi [29], ICLOCS2 [30], and Yop [31]. However, the time-optimal control problem in the 4th or higher-order is non-convex in discrete time, leading to high computational time and failure in obtaining optimal solutions. Leomanni et al. [32] transformed the time-optimal problem into sequential convex optimization problems, but the resulting trajectory exhibits serious oscillations. Solving the time-optimal problem for high-order chain-of-integrators systems efficiently and accurately is still challenging.

Quasi-optimal trajectories, especially those in the S-curve form, are widely used in industry. Erkorkmaz et al. [33] applied jerk-limited trajectories in the S-curve form in high-speed CNC machining. Dai et al. [34] planned snap-limited trajectories by solving motion time in S-curves. Ezair et al. [35] proposed a greedy recursive trajectory planning method for the high-order problem with full state constraints, but the method would fail for cases where the terminal position is close to the initial position, and the terminal velocity is far from the initial velocity. Oland et al. [36] planned suboptimal 4th order trajectories without any constraints to obtain a zero terminal based on exponential activation functions. However, the current methods either underutillize the inertia of system states or fall short of attaining full state constraints, thereby leading to unsatisfactory in motion time.

This paper theoretically studies the time-optimal control problem for high-order chain-of-integrators systems with full state constraints and arbitrary initial as well as terminal states. A novel notation system and theoretical framework is established in Section III, providing key concepts, i.e., the switching law and the optimal-trajectory manifold. A trajectory planning method named the manifold-intercept method (MIM) is proposed in Section IV and is open-source in [37]. The contributions of this paper include the following aspects:

1) This paper establishes a novel notation system and theoretical framework for the classical and longstanding problem in optimal control, i.e., the time-optimal control problem for high-order chain-of-integrators systems. Through comprehensive analysis of states and costates, the framework can provide the switching manifold for high-order problems in the form of switching laws. Notably, limited studies on the switching hypersurface have been conducted even for 4th order problems. This paper derives properties of switching laws regarding signs as well as dimension and proposes a definite condition of augmented switching laws, imposing a necessary condition on optimal control for directly solving the nonlinear equation system.
2) Guided by the developed framework, this paper proposes an efficient trajectory planning algorithm called manifold-intercept method (MIM). The proposed MIM can plan near-time-optimal trajectories for 4th or higher-order problems with only negligible extra motion time compared to time-optimal trajectories, avoiding chattering in high-order problems with near-optimal terminal time compared to optimal solutions. The proposed MIM outperforms all baselines on computational time, computational accuracy, and trajectory quality by a large gap. To the best of our knowledge, there has been no mature method available for planning 4th order optimal trajectories with full state constraints so far.
3) For 3rd order problems, the proposed MIM can plan strictly time-optimal trajectories with full state constraints. According to the available literature, the proposed MIM is the first 3rd order trajectory planning method with full state constraints and arbitrary terminal states. While it is claimed that Ruckig in pro version [38] can achieve 3rd order trajectories with full state constraints, it is neither open-source nor explicit publishes its underlying principles. Since 3rd order trajectories are widely applied in the industry [1], [26], the proposed algorithm has significant application value.

II. Problem Formulation

As mentioned in Section I, time-optimal control for chain-of-integrator systems is a classical problem in the optimal control theory domain, remaining challenging to plan trajectories with input saturation, full state constraints [11], and arbitrary terminal states [18], [19]. Generally, the problem can be summarized as

$$\min \quad J = \int_0^{t_\mathrm{f}} \mathrm{d}t = t_\mathrm{f}, \tag{1a}$$

$$\text{s.t.} \quad \dot{x}_k(t) = x_{k-1}(t), \forall t \in [0, t_\mathrm{f}], k = 2, 3, \ldots, n, \tag{1b}$$

$$\dot{x}_1(t) = u(t), \forall t \in [0, t_\mathrm{f}], \tag{1c}$$

$$\boldsymbol{x}(0) = \boldsymbol{x}_0,\ \boldsymbol{x}(t_\mathrm{f}) = \boldsymbol{x}_\mathrm{f}, \tag{1d}$$

$$|x_k(t)| \le M_k,\ \forall t \in [0, t_\mathrm{f}],\ k = 1, 2, \ldots, n, \tag{1e}$$

$$|u(t)| \le M_0,\ \forall t \in [0, t_\mathrm{f}], \tag{1f}$$

where $\boldsymbol{x} = (x_1, x_2, \ldots, x_n) \in \mathbb{R}^n$ is the state vector of the system, $u \in \mathbb{R}$ is the control input. $\boldsymbol{x}_0 = (x_{01}, x_{02}, \ldots, x_{0n})$ and $\boldsymbol{x}_\mathrm{f} = (x_{\mathrm{f}1}, x_{\mathrm{f}2}, \ldots, x_{\mathrm{f}n})$ are the assigned initial state vector and terminal state vector. n is called the order of problem (1). The notation $(\bullet)$ means $[\bullet]^\top$.

Problem (1) possesses a clear physical significance. For example, if $n = 4$, x_4, x_3, x_2, x_1, and u represent the position, velocity, acceleration, jerk, and snap of a 1-axis motion system, respectively. Then, (1) requires planning a trajectory with minimum motion time from a given initial state vector to a terminal state vector under box constraints.

For the convenience, denote $\boldsymbol{M} = (M_0, M_1, \dots, M_n) \in \mathbb{R}_{++} \times \overline{\mathbb{R}}_{++}^n$, where $\overline{\mathbb{R}}_{++} = \mathbb{R}_{++} \cup \{\infty\}$ is the strictly positive part of the extended real number line. $M_k = \infty$ if x_k is unconstrained. Problem (1) is denoted as $\mathcal{P}(\boldsymbol{x}_0, \boldsymbol{x}_\mathrm{f}; \boldsymbol{M})$.

In order to solve the optimal control problem (1), the Hamiltonian is constructed as

$$\begin{aligned} &\mathcal{H}(\boldsymbol{x}(t), u(t), \lambda_0, \boldsymbol{\lambda}(t), \boldsymbol{\eta}(t), t) \\ =&\lambda_0 + \lambda_1 u + \sum_{k=2}^{n} \lambda_k x_{k-1} + \sum_{k=1}^{n} \eta_k (|x_k| - M_k), \end{aligned} \tag{2}$$

where $\lambda_0 \geq 0$. $\boldsymbol{\lambda}(t) = (\lambda_1(t), \lambda_2(t), \dots, \lambda_n(t)) \in \mathbb{R}^n$ is the costate vector, and $(\lambda_0, \boldsymbol{\lambda}(t)) \neq 0$. $\boldsymbol{\lambda}$ satisfies the Hamilton's equations [39]:

$$\dot{\lambda}_k = -\frac{\partial \mathcal{H}}{\partial x_k},\ k = 1, 2, \cdots, n, \tag{3}$$

i.e.,

$$\begin{cases} \dot{\lambda}_k = -\lambda_{k+1} - \eta_k \operatorname{sgn}(x_k),\ k < n, \\ \dot{\lambda}_n = -\eta_n \operatorname{sgn}(x_n). \end{cases} \tag{4}$$

The initial costates $\boldsymbol{\lambda}(0)$ and the terminal costates $\boldsymbol{\lambda}(t_\mathrm{f})$ are not assigned since $\boldsymbol{x}(0)$ and $\boldsymbol{x}(t_\mathrm{f})$ are given in problem (1).

In (2), $\boldsymbol{\eta}$ is the multiplier vector induced by inequality constraints (1e), satisfying

$$\eta_k \geq 0,\ \eta_k (|x_k| - M_k) = 0,\ k = 1, 2, \cdots, n. \tag{5}$$

Equivalently, $\forall t \in [0, t_\mathrm{f}]$, $\eta_k(t) \neq 0$ only if $|x_k(t)| = M_k$.

PMP gives the results that the input control $u(t)$ minimizes the Hamiltonian $\mathcal{H}$ [12], i.e.,

$$u(t) \in \underset{|U| \leq M_0}{\arg\min}\, \mathcal{H}(\boldsymbol{x}(t), U, \lambda_0, \boldsymbol{\lambda}(t), \boldsymbol{\eta}(t), t). \tag{6}$$

Therefore,

$$u(t) = \begin{cases} M_0, & \lambda_1(t) < 0 \\ *, & \lambda_1(t) = 0 \\ -M_0, & \lambda_1(t) > 0 \end{cases}, \tag{7}$$

where $u(t)$ is undetermined during $\lambda_1(t) = 0$. Evidently, the value of $u(t)$ in a zero-measure set have no influence on the integral result. However, a singular condition occurs when $\lambda_1(t) = 0$ holds for a period of time. The control law for the 3rd order version of (7) was previously reasoned and named the Bang-Singular-Bang time-optimal control law in [11].

The continuity of the system is guaranteed in two folds. On one hand,

$$\forall t \in [0, t_\mathrm{f}],\ \mathcal{H}(\boldsymbol{x}(t), u(t), \lambda_0, \boldsymbol{\lambda}(t), \boldsymbol{\eta}(t), t) \equiv 0 \tag{8}$$

holds along the time-optimal trajectory. On the other hand, the junction condition [12], [40] is reasoned from the necessary conditions for optimality. More specifically, $\boldsymbol{\lambda}$ might jump when the state vector $\boldsymbol{x}$ enters or exits the boundaries of the inequality constraints (1e). In other words, $\boldsymbol{\lambda}$ might not be continuous when $\boldsymbol{x}$ switches between $|x_k| < M_k$ and $|x_k| = M_k$ for some k.

III. System Behavior Analysis and Switching Laws for the Time-Optimal Control Problem

Section II has provided the problem form and some properties of system states and costates. The Bang-Singular-Bang control law (7) indicates the importance of the costate analysis. Section III-A and Section III-B analyze costates and system behaviors, respectively. Then, system behaviors of problem (1) are classified into finite ones and the theory of the switching law is developed in Section III-C. Finally, the definite condition of problem (1) is induced by the proposed augmented switching law in Section III-D.

A. Jump Condition of Costates $\boldsymbol{\lambda}$

As mentioned in Section II, the costate vector $\boldsymbol{\lambda}$ might not be continuous at the connection of unconstrained arcs and constrained boundary, i.e., $|x_k|$ increases onto M_k or decreases from M_k for some k. The above behavior is called the junction condition (or jump condition) of costates [41]. The junction condition has a significant influence on the switching law of the optimal control u.

Assume the junction condition for $|x_k| \leq M_k$ occurs at time t_1. According to [41], $\exists \mu \leq 0$, s.t.

$$\boldsymbol{\lambda}(t_1^+) - \boldsymbol{\lambda}(t_1^-) = \mu \frac{\partial (|x_k| - M_k)}{\partial \boldsymbol{x}} = \mu \operatorname{sgn}(x_k) \boldsymbol{e}_k, \tag{9}$$

where the k-th component of $\boldsymbol{e}_k \in \mathbb{R}^n$ is 1, and other components of $\boldsymbol{e}_k$ are 0. In other words, $\forall i \neq k$, λ_i is continuous at t_1, while λ_k might jump at t_1.

Two cases for the junction condition exist: (a) $|x_k| \equiv M_k$ for a period of time, i.e., the connection of an unconstrained arc and a constrained arc; (b) $|x_k|$ touches M_k at a single time point i.e., the connection of two unconstrained arcs at the constrained boundary. The above two cases will be discussed in Section III-A1 and Section III-A2. Among them, Case 1 induces the system behavior defined in Definition 1, while Case 2 induces the tangent marker in Definition 8. The limit point of chattering phenomena in problem (1), in a one-sided neighborhood of which $|x_k| = M_k$ and $|x_k| < M_k$ occur for infinite times, i.e., unconstrained arcs are connected at the constrained boundary with lengths converging to 0, will be investigated in our related work [42].

1) Case 1. $|x_k| \equiv M_k$ for A Period of Time:

Without loss of generality, assume that $\forall t \in [t_1, t_2]$, $x_k(t) \equiv M_k$, and $\exists \delta > 0$, $\forall t \in (t_1 - \delta, t_1)$, $x_k(t) < M_k$. The case where x_k leaves M_k or $x_k \equiv -M_k$ is similar.

For $t \in [t_1, t_2]$, $x_k \equiv M_k$, $\dot{x}_1 = u$, and $\forall i < k$, $\dot{x}_{i+1} = x_i$. Hence, $u \equiv 0$ and $\forall i < k$, $x_i \equiv 0$. Note that $\forall i > k$, $x_i(t)$ is a polynomial of degree $(i-k)$, and $\left|\frac{\mathrm{d}^{(i-k)} x_i}{\mathrm{d}t^{(i-k)}}\right| \equiv M_k \neq 0$. So $|x_i| = M_i$ holds at most for $2(i-k)$ number of points. In other words, $\forall i > k$, $|x_i| < M_i$ holds except at finite time points. From (5) and (7), $\lambda_1 \equiv 0$, and $\forall i \neq k$, $\eta_i \equiv 0$ almost everywhere. It can be reasoned from (4) that $\forall i \leq k$, $\lambda_i \equiv 0$. The term "almost everywhere" means a proposition holds for all points except for a zero-measure set [43].

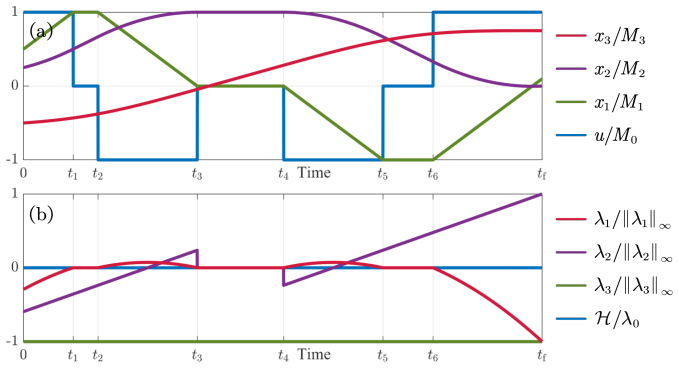

Fig. 2. A 3rd order optimal trajectory represented by $\overline{01}0\overline{2}01\overline{0}$ in this paper, where $\lambda_0 > 0$. (a) The state vector. (b) The costate vector.

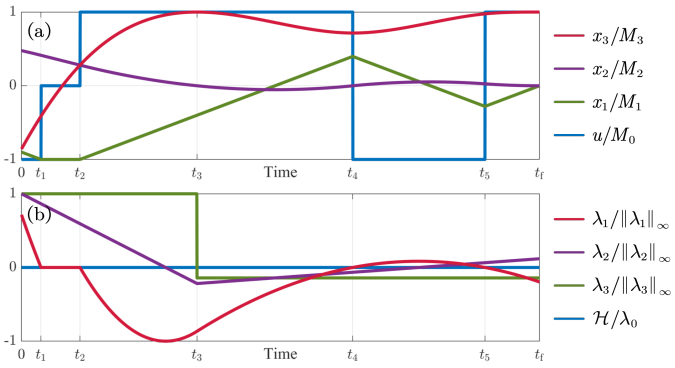

Fig. 3. A 3rd order optimal trajectory represented by $\underline{01}\overline{0}\,(\overline{3},2)\,\overline{0}\underline{0}\overline{0}$ in this paper, where $\lambda_0 > 0$. (a) The state vector. (b) The costate vector.

Furthermore, in the case where $k = 1$, λ_1 keeps continuous despite the junction condition (9). According to (8),

$$\mathcal{H}^{\pm} = \lambda_0 + \lambda_1^{\pm} u^{\pm} + \sum_{l=2}^{n} \lambda_l x_{l-1} = 0. \tag{10}$$

From $\mathcal{H}^+ = \mathcal{H}^-$, $\lambda_1^+ u^+ = \lambda_1^- u^-$. The notation $\bullet^{\pm}$ means the left and right-hand limits of variable $\bullet$ at the junction time. Note that $u^+ = 0$, $u^- = M_0$, $\lambda_1^+ = 0$, so $\lambda_1^- = 0$. Therefore, $\lambda_1^+ = \lambda_1^- = 0$, i.e., λ_1 keeps continuous at the junction time.

Noted that the case where $|x_n| \equiv M_n$ for a period of time does not exist. By contradiction, if $\exists t_1 < t_2$, s.t. $\forall t \in [t_1, t_2]$, $|x_n(t)| \equiv M_n$, then $x_1(t) = x_2(t) = \cdots = x_{n-1}(t) = 0$ for $t \in [t_1, t_2]$. In other words, the system state vector $\boldsymbol{x}$ parks at $\pm M_n \boldsymbol{e}_n$ for a period of time, which contradicts the time-optimality. As a corollary, (4) can be written as

$$\begin{cases} \dot{\lambda}_l = -\lambda_{l+1} - \eta_l \operatorname{sgn}(x_l), \, l < n, \\ \dot{\lambda}_n = 0, \end{cases} \tag{11}$$

since $\eta_n = 0$ almost everywhere. It should be pointed out that λ_n might not be constant though $\dot{\lambda}_n = 0$, because λ_n might jump when $|x_n|$ touches M_n in the following Case 2.

An example of Case 1 is shown in Fig. 2. $|x_1| \equiv M_1$ for $t \in [t_1, t_2] \cup [t_5, t_6]$, but λ_1 keeps continuous despite to the junction condition (9). $x_2 \equiv M_2$ for $t \in [t_3, t_4]$, and λ_2 jumps decreasingly at t_3 and t_4.

2) Case 2. $|x_k|$ Touches M_k at A Single Time Point:

Without loss of generality, assume that x_k touches M_k at t_1, i.e., $x_k(t_1) = M_k$, and $\exists \delta > 0$, $\forall t \in (t_1 - \delta, t_1) \cup (t_1, t_1 + \delta)$, $x_k(t) < M_k$. The case where x_k touches $-M_k$ can be reasoned similarly.

The case where $k = 1$ is evident to Case 1 in Section III-A1. Without loss of generality, assume x_1 touches M_1 at t_1. $\exists \varepsilon > 0$, $\forall t \in (0, \varepsilon)$, $u(t_1 + t) < 0$, while $u(t_1 - t) > 0$. By (7), $\forall t \in (0, \varepsilon)$, $\lambda_1(t_1 - t) \le 0 \le \lambda_1(t_1 + t)$; hence, $\lambda_1(t_1^+) \ge \lambda_1(t_1^-)$. (9) indicates that $\lambda_1(t_1^+) - \lambda_1(t_1^-) \le 0$. So $\lambda_1(t_1^+) = \lambda_1(t_1^-) = 0$, i.e., λ_1 keeps continuous at t_1.

In the case where $k \ge 2$, $\exists \varepsilon \in (0, \delta)$, s.t. $\forall t \in (0, \varepsilon)$, $u(t_1 + t) \equiv u^+$, and $u(t_1 - t) \equiv u^-$. (a) If $x_{k-1} = x_{k-2} = \cdots = x_1 = 0$ at t_1, then $\forall t \in (0, \varepsilon)$, $x_k(t_1 + t) = M_k + \frac{u^+}{k!} t^k < M_k$, and $x_k(t_1 - t) = M_k + \frac{u^-}{k!}(-t)^k < M_k$. Then, $u^+ = -M_0$, $u^- = (-1)^{k-1} M_0$. (b) If $\exists i = 1, 2, \ldots, k-1$, $x_i(t_1) \ne 0$, then let $h^* = \operatorname{argmin}\{h : x_{k-h}(t_1) \ne 0\} > 1$, noting that $x_{k-1}(t_1) = \frac{\mathrm{d}x_k}{\mathrm{d}t}\big|_{t=t_1} = 0$. Since x_{k-h^*} is continuous, $\exists \tilde{\varepsilon} \in (0, \varepsilon)$, $\forall t \in (-\tilde{\varepsilon}, \tilde{\varepsilon})$, $|x_{k-h^*}(t_1 + t) - x_{k-h^*}(t_1 + t)| < \frac{1}{2}|x_{k-h^*}(t_1)|$; hence, $\operatorname{sgn}(x_{k-h^*}(t_1 + t)) \equiv \operatorname{sgn}(x_{k-h^*}(t_1))$. By Taylor expansions of x_k at t_1, $\forall t \in [-\tilde{\varepsilon}, \tilde{\varepsilon}]$, $\exists \theta_t \in (0, 1)$, $x_k(t_1 + t) - x_k(t_1) = \frac{t^{h^*}}{h^*!} x_{k-h^*}(t_1 + \theta_t t) < 0$. Therefore, $x_{k-h^*}(t_1) < 0$ and h^* is even.

For cases where (a) $n \le 2$, and where (b) $n = 3$ with $M_3 = \infty$, there exist costate vectors for optimal trajectories which do not jump when Case 2 occurs, noting that the costate vector can be non-unique for one optimal solution. In the case where $n = 3$ with $M_3 < \infty$, the jerk-limited time-optimal problem under position constraints is still not well solved yet. He et al. [11] developed the analytic expression of switching surfaces in 3rd order with zero terminal states, where Case 2, fortunately, does not exist with zero terminal states. Reflexxes [18] and Ruckig in community version [19], the two most famous open-source online trajectory planning packages, are not able to plan jerk-limited trajectories under position constraints.

An example of Case 2 is shown in Fig. 3. Though $\dot{\lambda}_3 \equiv 0$ almost everywhere, λ_3 jumps at t_3 since x_3 touches M_3 at t_3. Two critical corollaries based on analysis above are as follows:

Proposition 1 (Bang-Singular-Bang Control Law)**.** *The optimal control $u(t)$ of* (1) *satisfies*

$$u(t) = \begin{cases} M_0, & \lambda_1(t) < 0 \\ 0, & \lambda_1(t) = 0 \\ -M_0, & \lambda_1(t) > 0 \end{cases} \quad \textit{almost everywhere.} \tag{12}$$

Proof. $\lambda_1(t) \equiv 0$ occurs only if $\exists k$, s.t. $|x_k(t)| \equiv M_k$, or else $\boldsymbol{\lambda}(t) \equiv \boldsymbol{0}$. If $\boldsymbol{\lambda}(t) \equiv \boldsymbol{0}$, then (8) implies that $\lambda_0 = 0$, which contradicts $(\lambda_0, \boldsymbol{\lambda}(t)) \ne 0$. Therefore, $u(t) \equiv 0$ if $\lambda_1(t) \equiv 0$. Hence, (12) is equivalent to (7) almost everywhere. □

Proposition 2. *If* (1) *has an optimal control, then the optimal control is unique in an almost everywhere sense. In other words, if $u = u_1^*(t)$ and $u = u_2^*(t)$, $t \in [0, t_\mathrm{f}^*]$, are both the optimal control of* (1)*, then $u_1^*(t) = u_2^*(t)$ almost everywhere.*

Proof. Denote μ as the Lebesgue measure [43] on $\mathbb{R}$, and $Q_1 \triangleq \{t : u_1^*(t), u_2^*(t) \in \{0, \pm M_0\}\}$. From Proposition 1, $\mu(Q_1) = t_\mathrm{f}^*$. Let $Q_2 \triangleq \{t : u_1^*(t) \ne u_2^*(t)\}$. If $\mu(Q_2) > 0$,

then denote $u_3^*(t) = \frac{1}{4}u_1^*(t) + \frac{3}{4}u_2^*(t)$, $t \in [0, t_\mathrm{f}^*]$. It can be verified that $u_3^*(t)$ is also an optimal control of problem (1). However, $\forall t \in Q_1 \cap Q_2$, $u_3^*(t) \notin \{0, \pm M_0\}$; hence, $0 = \mu\{u_3^*(t) \notin \{0, \pm M_0\}\} > \mu(Q_1 \cap Q_2) = \mu(Q_2) > 0$, which contradicts Proposition 1. Therefore, $\mu(Q_2) = 0$. □

B. System Behavior

The case where the inequality constraints (1e) hold strictly, i.e., $\forall k$, $|x_k| < M_k$, is first considered. In this case, it is evident that $\boldsymbol{\lambda}$ does not jump and $\boldsymbol{\eta} \equiv \mathbf{0}$ in this period. Therefore,

$$\begin{cases} \dot{\lambda}_k = -\lambda_{k+1},\ k < n \\ \dot{\lambda}_n = 0 \end{cases},\ \text{if } \forall t \in [t_1, t_2],\ |\boldsymbol{x}(t)| < \boldsymbol{M}. \quad (13)$$

Since $\boldsymbol{\lambda}$ is continuous, (13) indicates that $\lambda_k(t)$ is an $(n-k)$-th degree polynomial for $t \in [t_1, t_2]$. According to the fundamental theorem of algebra [43], λ_k has no more than $(n-k)$ roots for $t \in [t_1, t_2]$. A corollary, also well-known in previous works [13], is reasoned as follows:

Proposition 3. *Assume $\forall t \in [t_1, t_2]$, $\forall k$, $|x_k(t)| < M_k$ in problem (1). Then, the optimal control u switches between M_0 and $-M_0$ with no more than $(n-1)$ times in $[t_1, t_2]$.*

Proof. If $\forall t \in [t_1, t_2]$, $\forall k$, $|x_k| < M_k$, then $\boldsymbol{\lambda}$ is continuous. Specifically, $\lambda_n \equiv \mathrm{const}$. By (13), λ_1 is an $(n-1)$-th degree polynomial for $t \in [t_1, t_2]$. Note that $\lambda_1 \equiv 0$ contradicts (8) when $\boldsymbol{\eta} \equiv 0$. Therefore, λ_1 has no more than $(n-1)$ roots. According to Proposition 1, u switches between M_0 and $-M_0$ with no more than $(n-1)$ times. □

The properties of states and costates reasoned in Section III-A and Section III-B are summarized as follows:

Theorem 1. *The following propositions hold for the optimal control of problem (1).*

1) $u(t) = -\mathrm{sgn}(\lambda_1(t))M_0$ *almost everywhere. Specifically, $u(t) \equiv 0$ if $\lambda_1(t) \equiv 0$.*
2) $\forall t \in [0, t_\mathrm{f}]$, $\boldsymbol{\lambda}(t) \neq \mathbf{0}$.
3) *λ_1 and $\boldsymbol{x}$ are continuous, while $\lambda_k\ (k > 1)$ might jump at junction time.*
4) *λ_k consists of $(n-k)$-th degree polynomials and zero. Specifically, $\lambda_1 \equiv 0$ for a period of time if and only if $\exists k, |x_k| \equiv M_k$ during the period of time.*
5) *For $k < n$, cases might exist where $\exists t_1 < t_2, \delta > 0$, s.t. $\forall t \in [t_1, t_2]$, $|x_k(t)| \equiv M_k$, while $\forall t \in (t_1 - \delta, t_1) \cup (t_2, t_2 + \delta)$, $|x_k(t)| < M_k$. Then, $\forall t \in [t_1, t_2]$,*
   a) *$\forall i \leq k$, $\lambda_i(t) \equiv 0$, while $\forall i > k$, $\lambda_i(t)$ is an $(n-i)$-th degree polynomial. Furthermore, $\lambda_{k+1}(t)$ is not always zero.*
   b) *$u(t) \equiv 0$. $\forall i < k$, $x_i(t) \equiv 0$.*
   c) *$\forall i \neq k$, λ_i is continuous. Only if $1 < k < n$, λ_k might jump at t_1 and t_2.*
6) *For $k > 2$, case might exist where $\exists t_1 \in (0, t_\mathrm{f})$, $\delta > 0$, s.t. $|x_k(t_1)| = M_k$, while $\forall t \in (t_1 - \delta, t_1) \cup (t_1, t_1 + \delta)$, $|x_k(t)| < M_k$. Then, λ_k might jump at t_1, and one and only one of the following cases holds:*
   a) *$\exists l < \frac{k}{2}$, s.t. $x_{k-1} = x_{k-2} = \cdots = x_{k-2l+1} = 0$ at t_1, while $x_{k-2l}(t_1) \neq 0$, and $\mathrm{sgn}(x_{k-2l}(t_1)) = -\mathrm{sgn}(x_k(t_1))$. Denote $h = 2l$ as the degree of $|x_k(t_1)| = M_k$.*
   b) *$x_{k-1} = x_{k-2} = \cdots = x_1 = 0$ at t_1. $u(t_1^+) = -\frac{M_0}{M_k}x_k(t_1)$, and $u(t_1^-) = (-1)^{k-1}\frac{M_0}{M_k}x_k(t_1)$. Denote $h = k$ as the degree of $|x_k(t_1)| = M_k$.*

Proof. Based on discussion in Section III-A and Section III-B, Theorem 1 is evident. □

Theorem 1 fully lists system behaviors in a single stage of a sub-arc without limit points of chattering phenomena in an optimal trajectory, since connections between unconstrained arcs or constrained arcs at constrained boundaries with positive length have been fully discussed. The system behavior is classified into finite ones and is proposed formally as follows:

Definition 1. System behavior of problem (1) at a single stage is denoted as follows:

1) The stage where $u \equiv M_0$ $(-M_0)$ is denoted as $\overline{0}$ $(\underline{0})$.
2) The stage where $x_k \equiv M_k\ (-M_k), u \equiv 0$, and $\forall i < k, x_i \equiv 0$, is denoted as $\overline{k}$ $(\underline{k})$.
3) $\forall 0 \leq k \leq n$, the signs of $\overline{k}$ and $\underline{k}$ are denoted by $\mathrm{sgn}(\overline{k}) = 1$, $\mathrm{sgn}(\underline{k}) = -1$. The value of $\overline{k}$ and $\underline{k}$ is denoted as $|\overline{k}| = |\underline{k}| = k$.

Based on Theorem 1 and Definition 1, system behaviors during the whole moving process can be studied. In the following, the sign of a system behavior can be left out if no ambiguity exists.

C. Switching Law and Optimal-Trajectory Manifold

Building on the analysis of the system behavior in Section III-A and Section III-B, this section focuses on how the system behavior switches along the time-optimal trajectory. The core idea in this section is the switching law and the optimal-trajectory manifold for time-optimal control, which are defined in Section III-C1. The properties of the switching law on dimension and sign are reasoned in Section III-C2 and Section III-C3, respectively.

1) Definitions:

Definition 2. Given a problem $\mathcal{P}$, assume the time-optimal trajectory passes through system behaviors $s_1, s_2, \ldots, s_N$ successively. Then, the series of system behaviors $S = s_1 s_2 \cdots s_N$ is called the **switching law** w.r.t. $\mathcal{P}$, denoted as $S = \mathcal{S}(\mathcal{P})$, where $N \in \mathbb{N}^*$ is called the length of S.

The switching law of a problem is unique according to Proposition 2. As an example, two second order optimal problems with the same terminal state vector are shown in Fig. 4. The switching law of $\mathcal{P}_1 = \mathcal{P}\left(\boldsymbol{x}_0^{(1)}, \boldsymbol{x}_\mathrm{f}; \boldsymbol{M}\right)$ is $\mathcal{S}(\mathcal{P}_1) = \underline{0}1\overline{0}$. In other words, along the time-optimal trajectory from $\boldsymbol{x}_0^{(1)}$ to $\boldsymbol{x}_\mathrm{f}$, $\exists 0 < t_1 < t_2 < t_3 < t_\mathrm{f}$, s.t.

1) $\underline{0}$: $\forall t \in (0, t_1), u(t) \equiv -M_0$. $\boldsymbol{x}$ starts from $\boldsymbol{x}(0) = \boldsymbol{x}_0^{(1)}$, and x_1 enters $-M_1$ at t_1.
2) $\underline{1}$: $\forall t \in (t_1, t_2), x_1(t) \equiv -M_1$, while $u(t) \equiv 0$.
3) $\overline{0}$: $\forall t \in (t_2, t_\mathrm{f}), u(t) \equiv M_0$. x_1 exits $-M_1$ at t_2, and the system state vector $\boldsymbol{x}$ reaches the terminal state vector $\boldsymbol{x}_\mathrm{f}$ at t_f.

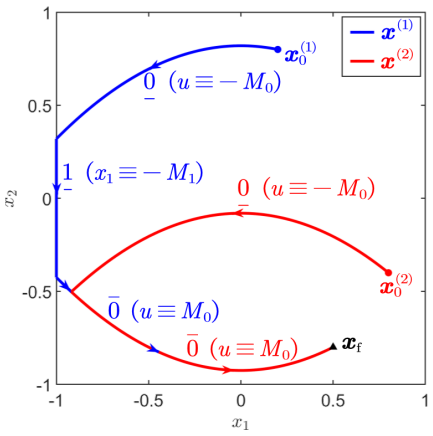

Fig. 4. Switching laws for 2 optimal problems with the same terminal state vector $\boldsymbol{x}_\mathrm{f}$, i.e., $\mathcal{P}_1 = \mathcal{P}\left(\boldsymbol{x}_0^{(1)}, \boldsymbol{x}_\mathrm{f}; \boldsymbol{M}\right)$ and $\mathcal{P}_2 = \mathcal{P}\left(\boldsymbol{x}_0^{(2)}, \boldsymbol{x}_\mathrm{f}; \boldsymbol{M}\right)$. Among them, $n = 2$, $\boldsymbol{M} = (1, 1, 1)$, $\mathcal{S}(\mathcal{P}_1) = \underline{1}\bar{0}$, and $\mathcal{S}(\mathcal{P}_2) = \underline{0}\bar{0}$.

A similar analysis applies to $\mathcal{P}_2 = \mathcal{P}\left(\boldsymbol{x}_0^{(2)}, \boldsymbol{x}_\mathrm{f}; \boldsymbol{M}\right)$. From examples shown in Fig. 4, it can be observed that the switching law depends on the initial states.

Notably, a switching law focuses on how the system behavior switches along the trajectory, without information on motion time. The optimal control of problem (1) consists of a switching law and motion time for every system behavior, whose definite conditions will be discussed in Section III-D.

For an n-th order problem (1), a natural approach is to employ mathematical induction, utilizing the solutions of lower-order problems to solve the n-th order problem. The above idea induces the definitions of the sub-problem and optimal-trajectory manifold.

For the convenience of discussion, the optimal trajectory, the optimal control, and the terminal time of a problem $\mathcal{P}$ are denoted by $\boldsymbol{x}^*(t; \mathcal{P})$, $u^*(t; \mathcal{P})$, and $t_\mathrm{f}^*(\mathcal{P})$, respectively.

Definition 3. For an n-th order problem $\mathcal{P} = \mathcal{P}(\boldsymbol{x}_0, \boldsymbol{x}_\mathrm{f}; \boldsymbol{M})$ and $0 \le a_i \le b_i \le n$, $a_1, a_2 \ge 1$, a **sub-problem** of $\mathcal{P}$ is $\hat{\mathcal{P}} = \mathcal{P}\left(\boldsymbol{x}_0^{a_1:b_1}, \boldsymbol{x}_\mathrm{f}^{a_2:b_2}; \boldsymbol{M}^{a_3:b_3}\right)$, i.e., the time-optimal problem for chain-of-integrators with the following constraints:

$$\begin{cases} x_k(0) = x_{0k}, & a_1 \le k \le b_1 \\ x_k(t_\mathrm{f}) = x_{\mathrm{f}k}, & a_2 \le k \le b_2, \\ |x_k| \le M_k, & a_3 \le k \le b_3. \end{cases} \tag{14}$$

Definition 4. Two time-optimal problems $\mathcal{P}_1, \mathcal{P}_2$ are **equivalent**, denoted as $\mathcal{P}_1 \Leftrightarrow \mathcal{P}_2$, if $\mathcal{P}_1$ and $\mathcal{P}_2$ have the same solution of optimal control, i.e.,

$$\begin{cases} t_\mathrm{f}^*(\mathcal{P}_1) = t_\mathrm{f}^*(\mathcal{P}_2), \\ u^*(t, \mathcal{P}_1) = u^*(t, \mathcal{P}_2) \text{ almost everywhere.} \end{cases} \tag{15}$$

The equivalence between two problems is well-defined since the optimal for each problem is unique, according to Proposition 2. Two problems are equivalent when their boundary conditions can replace each other. Specifically, if a problem $\mathcal{P}$ is equivalent to its sub-problem $\hat{\mathcal{P}}$, then some boundary conditions and constraints of $\mathcal{P}$ is unnecessary. The above observation contributes to the following definition:

Definition 5. Given $\boldsymbol{x}_\mathrm{f} \in \mathbb{R}^n$ and $\boldsymbol{M} \in \mathbb{R}_{++} \times \overline{\mathbb{R}}_{++}^n$, define

$$\mathcal{F}_k(\boldsymbol{x}_\mathrm{f}, \boldsymbol{M}) \triangleq \bigcup \{\boldsymbol{x}_0 \in \mathbb{R}^n : \mathcal{P}(\boldsymbol{x}_0, \boldsymbol{x}_\mathrm{f}; \boldsymbol{M}) \Leftrightarrow \mathcal{P}\left(\boldsymbol{x}_0^{1:k}, \boldsymbol{x}_\mathrm{f}^{1:k}; \boldsymbol{M}\right) \text{ are feasible}\} \tag{16}$$

as the k-th order **optimal-trajectory manifold** of $\boldsymbol{x}_\mathrm{f}$ under $\boldsymbol{M}$. Proposition 2 provides the well-posedness of $\mathcal{F}_k(\boldsymbol{x}_\mathrm{f}, \boldsymbol{M})$.

"$\Leftrightarrow$" is evidently an equivalence relation among the set of feasible time-optimal control problems, which ensures the well-definedness of (16). Intuitively, $\mathcal{F}_k(\boldsymbol{x}_\mathrm{f}, \boldsymbol{M})$ consists of time-optimal trajectories for k-th order sub-problem, with high-dimensional components of states additionally. Noting that differential properties of $\mathcal{F}_k(\boldsymbol{x}_\mathrm{f}, \boldsymbol{M})$ are not utilized in this work, this paper names it as a "manifold" to establish its geometric intuition as a hypersurface, as shown in Fig. 5. In fact, a stratified set [44] might be clearer to describe $\mathcal{F}_k(\boldsymbol{x}_\mathrm{f}, \boldsymbol{M})$, but it requires much further formulation. The following proposition indicates that elements in $\mathcal{F}_k(\boldsymbol{x}_\mathrm{f}, \boldsymbol{M})$ are uniquely determined by their first k components.

Proposition 4. *If $\boldsymbol{x}_0, \boldsymbol{y}_0 \in \mathcal{F}_k(\boldsymbol{x}_\mathrm{f}, \boldsymbol{M})$, $\forall i \le k$, $x_{0i} = y_{0i}$, then $\boldsymbol{x}_0 = \boldsymbol{y}_0$.*

Proof. By $\mathcal{P}(\boldsymbol{x}_0, \boldsymbol{x}_\mathrm{f}; \boldsymbol{M}) \Leftrightarrow \mathcal{P}(\boldsymbol{y}_0, \boldsymbol{x}_\mathrm{f}; \boldsymbol{M})$, denote the optimal control as u^*. Note that u^* drives $\boldsymbol{x}$ from $\boldsymbol{x}_0, \boldsymbol{y}_0$ to $\boldsymbol{x}_\mathrm{f}$; hence, (1b) and (1c) imply $\boldsymbol{x}_0 = \boldsymbol{y}_0$. □

Definition 6. Assume $\mathcal{F}_k(\boldsymbol{x}_\mathrm{f}, \boldsymbol{M}) \neq \varnothing$ in (16). The **switching-law representation** of $\mathcal{F}_k(\boldsymbol{x}_\mathrm{f}, \boldsymbol{M})$ is defined as

$$\mathcal{SF}_k(\boldsymbol{x}_\mathrm{f}, \boldsymbol{M}) = \bigcup_{\boldsymbol{x}_0 \in \mathcal{F}_k(\boldsymbol{x}_\mathrm{f}, \boldsymbol{M})} \{\mathcal{S}(\mathcal{P}(\boldsymbol{x}_0, \boldsymbol{x}_\mathrm{f}; \boldsymbol{M}))\}. \tag{17}$$

An example of the second order optimal-trajectory manifold is shown in Fig. 5(a). It is indicated in Fig. 5(a) that $\mathcal{SF}_2(\boldsymbol{0}, \boldsymbol{M}) = \{\bar{0}, \underline{0}\bar{0}, \underline{1}\bar{0}, \underline{0}1\bar{0}, \underline{0}, \bar{0}\underline{0}, \bar{1}\underline{0}, \bar{0}1\underline{0}\}$. Fig. 5(a) is corresponding to $\mathcal{F}_2(\boldsymbol{0}, \boldsymbol{M})$ in Fig. 5(b). It can be observed that $\mathcal{F}_2(\boldsymbol{0}, \boldsymbol{M}) \subset \mathcal{F}_3(\boldsymbol{0}, \boldsymbol{M})$ is a sub-manifold of 2 dimensions, which confirms the validity of Proposition 4. Furthermore, every switching law induces a sub-manifold, i.e., any given sub-manifold of $\mathcal{F}_k(\boldsymbol{x}_\mathrm{f}, \boldsymbol{M})$ can be represented by a subset of $\mathcal{SF}_k(\boldsymbol{x}_\mathrm{f}, \boldsymbol{M})$.

2) Dimension Property of the Switching Law:

The dimension analysis of the optimal-trajectory manifold is indispensable to solve the time-optimal problem (1). For a given switching law S, the motion time of every stage can be determined by solving equations as follows only if S is of n dimension, since the number of variables should equal the number of independent equations [45].

Theorem 2. *Given a switching law $S = s_1 s_2 \dots s_N \in \mathcal{SF}_k(\boldsymbol{x}_\mathrm{f}, \boldsymbol{M})$, assume that $\forall 1 \le i < j \le N+1$, if $|s_i|, |s_j| > 0$, then $\sum_{l=i+1}^{j-1} |s_l| + \min\{|s_i|, |s_j|\} < j - i$, where $|s_{N+1}| \triangleq n$. The dimension of S, defined as the number of variables minus the number of equations except $\boldsymbol{x}_0$, is*

$$\dim S = N - \sum_{i=1}^{N} |s_i|. \tag{18}$$

Furthermore, if $|s_i| \neq 0$, then $|s_{i-1}| = |s_{i+1}| = 0$.

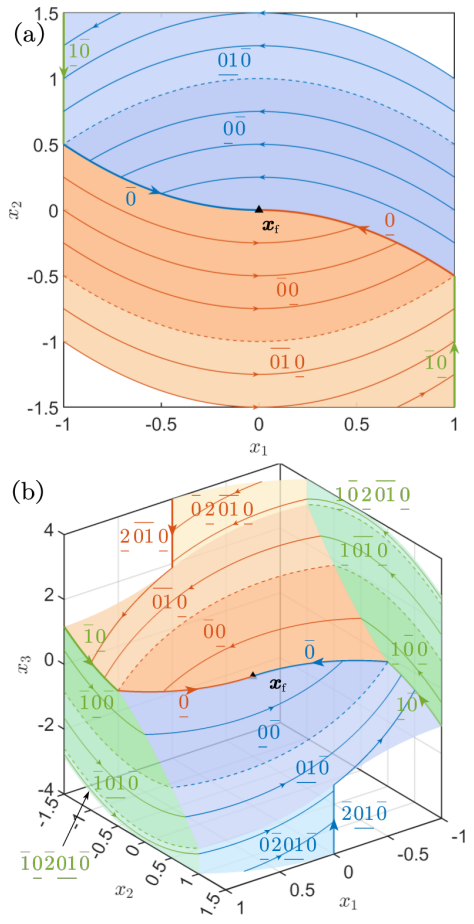

Fig. 5. Examples of the optimal-trajectory manifolds. (a) Second order. $\boldsymbol{M} = (1, 1, 1.5)$, $\boldsymbol{x}_\mathrm{f} = \boldsymbol{0}$. (b) Third order. $\boldsymbol{M} = (1, 1, 1.5, 4)$, $\boldsymbol{x}_\mathrm{f} = \boldsymbol{0}$. The parameters and the switching surfaces are the same as [11]. A structure similar to stratified sets [44] can be intuitively observed in the two examples.

Proof. Without loss of generality, assume $k = n$, or else it can be considered as $S \in \mathcal{SF}_k\left(\boldsymbol{x}_\mathrm{f}{}^{1:k}, \boldsymbol{M}\right)$ equivalently.

Assume $\boldsymbol{x}_i \in \mathbb{R}^n, i = 0, 1, \ldots, N$ and $t_i \geq 0, i = 1, 2, \ldots, N$. $\boldsymbol{x}_{i-1}$ moves to $\boldsymbol{x}_i$ after time t_i under the system behavior s_i, $\forall i = 1, 2, \ldots, N$. The terminal state vector $\boldsymbol{x}_N = \boldsymbol{x}_\mathrm{f}$ is given. Denote $\boldsymbol{x}_i = (x_{i,k})_{k=1}^n$. Note that $|s_N| = 0$.

Under the system behavior s_i, the control $u \equiv u_i$, where

$$u_i = \begin{cases} \operatorname{sgn}(s_i) M_0, & |s_i| = 0 \\ 0, & \text{otherwise} \end{cases}. \tag{19}$$

Under the system behavior $|s_i| = 0$, Nn constraints on state transformation exists, i.e., $\forall i = 1, 2, \ldots, N$, $l = 1, 2, \ldots, n$,

$$x_{i,l} = \sum_{j=1}^{l} \frac{1}{(l-j)!} x_{i-1,j} t_i^{l-j} + \frac{1}{l!} u_i t_i^l. \tag{20}$$

Under the system behavior $|s_i| \neq 0$, the states satisfy

$$\begin{cases} x_{i-1,j} = 0, j < |s_i| \\ x_{i-1,|s_i|} = \operatorname{sgn}(s_i) M_{|s_i|} \end{cases}, \forall i = 1, 2, \ldots, N-1. \tag{21}$$

(21) provides $\sum_{i=1}^N |s_i|$ constraints.

In summary, there exists $Nn + \sum_{i=1}^{N-1} |s_i|$ constraints and $(n+1)N$ variables in total. The independence of the above equations is proved in the extended version of this paper [46]. Therefore, the dimension of S is

$$\dim S = (n+1)N - \left(Nn + \sum_{i=1}^{N} |s_i|\right) = N - \sum_{i=1}^{N} |s_i|. \tag{22}$$

Assume $|s_i|, |s_{i-1}| \neq 0$. Note that $s_{i-1} \neq s_i$, and assume $|s_i| < |s_{i-1}|$. According to (21), $\left|x_{|s_i|}\left(T_i^+\right)\right| = M_{|s_i|}$, where T_i is the switching time between s_{i-1} and s_i. However, $x_{|s_i|}\left(T_i^-\right) = 0$; hence, $x_{|s_i|}$ is not continuous at T_i, which leads to a contradiction. Therefore, if $|s_i| \neq 0$, then $|s_{i-1}| = |s_{i+1}| = 0$. □

Intuitively, the dimension of a switching law characterizes the sub-manifold represented by the switching law. Take the optimal-trajectory manifold in Fig. 5(b) as an example. 0, 10, and 2010 are of 1 dimension. 00, 1010, and 02010 are of 2 dimensions. 000, 0010, and 0102010 are of 3 dimensions.

3) Sign Property of the Switching Law:

From Fig. 5(b), it is observed that $\underline{2\bar{0}1\bar{0}}$ exists while $\overline{2\bar{0}1\bar{0}}$ and $\underline{2\bar{0}1\bar{0}}$ do not exist. The analysis of the sign is given as the following theorem.

Theorem 3. $\forall S = s_1 s_2 \ldots s_N \in \mathcal{SF}_k(\boldsymbol{x}_\mathrm{f}, \boldsymbol{M})$, $\forall i = 2, 3, \ldots, N$,

$$\operatorname{sgn}(s_{i-1}) = \begin{cases} \operatorname{sgn}(s_i), & \text{if } |s_i| \text{ is odd} \\ -\operatorname{sgn}(s_i), & \text{if } |s_i| \text{ is even} \end{cases}. \tag{23}$$

Proof. In the case where $|s_{i-1}| = 0$, $|s_i| = 0$, note that $s_i \neq s_{i-1}$. Hence, $\operatorname{sgn}(s_{i-1}) = -\operatorname{sgn}(s_i)$.

In the case where $|s_{i-1}| \neq 0$, according to Theorem 2, $|s_i| = 0$. Denote the switching time between s_{i-1} and s_i as T_i. If $\operatorname{sgn}(s_{i-1}) = +1$, then $\forall k < |s_{i-1}|$, $x_k(T_i) = 0$ and $x_{|s_{i-1}|}(T_i) = M_{|s_{i-1}|}$. Assume that $\operatorname{sgn}(s_i) = +1$, i.e., $u \equiv u_i = M_0$ during s_i. Then, $\exists \delta > 0$, $\forall t \in (0, \delta)$, $x_{|s_{i-1}|}(T_i + t) = M_{|s_{i-1}|} + \frac{1}{|s_{i-1}|!} M_0 t^{|s_{i-1}|} > M_{|s_{i-1}|}$ since $u \equiv M_0$, which leads to a contradiction. Therefore, $\operatorname{sgn}(s_{i-1}) = +1$ if $\operatorname{sgn}(s_i) = -1$. For the similar analysis, $\operatorname{sgn}(s_{i-1}) = -1$ if $\operatorname{sgn}(s_i) = +1$.

In the case where $|s_i| \neq 0$, according to Theorem 2, $|s_{i-1}| = 0$. Denote the switching time between s_{i-1} and s_i as T_i. $x_k(T_i) = 0$ for $k < |s_i|$ and $x_{|s_i|}(T_i) = M_{|s_i|}$. Then, $\exists \delta > 0$, $\forall t \in (0, \delta)$, $u(T_i - t) \equiv \operatorname{sgn}(s_i) M_0$; hence, $x_{|s_i|}(T_i - t) = \operatorname{sgn}(s_i) M_{|s_i|} + \frac{1}{|s_i|!} M_0 t^{|s_i|} \cdot (-1)^{|s_i|} \operatorname{sgn}(s_{i-1})$. The constraint where $\left|x_{|s_i|}(T_i - t)\right| \leq M_{|s_i|}$ resulting that $(-1)^{|s_i|} \operatorname{sgn}(s_{i-1}) = -\operatorname{sgn}(s_i)$. □

Theorem 3 indicates that signs of all system behaviors in a switching law are uniquely determined by the sign of the last system behavior. For a switching law S of length N, Theorem 3 reduces the possible signs of all system behaviors from 2^N to 2.

D. Augmented Switching Law and Tangent Marker

For a given initial state vector $\boldsymbol{x}_0 \in \mathbb{R}^n$ and the switching law $S = \mathcal{S}(\mathcal{P}(\boldsymbol{x}_0, \boldsymbol{x}_\mathrm{f}; \boldsymbol{M}))$, Section III-C2 has pointed out that the optimal control can be solved only if $\dim S = n$. For example, in Fig. 5(a), $\boldsymbol{x}_0 \in \mathbb{R}^2$ is given. If $S = \bar{0}\underline{0}$,

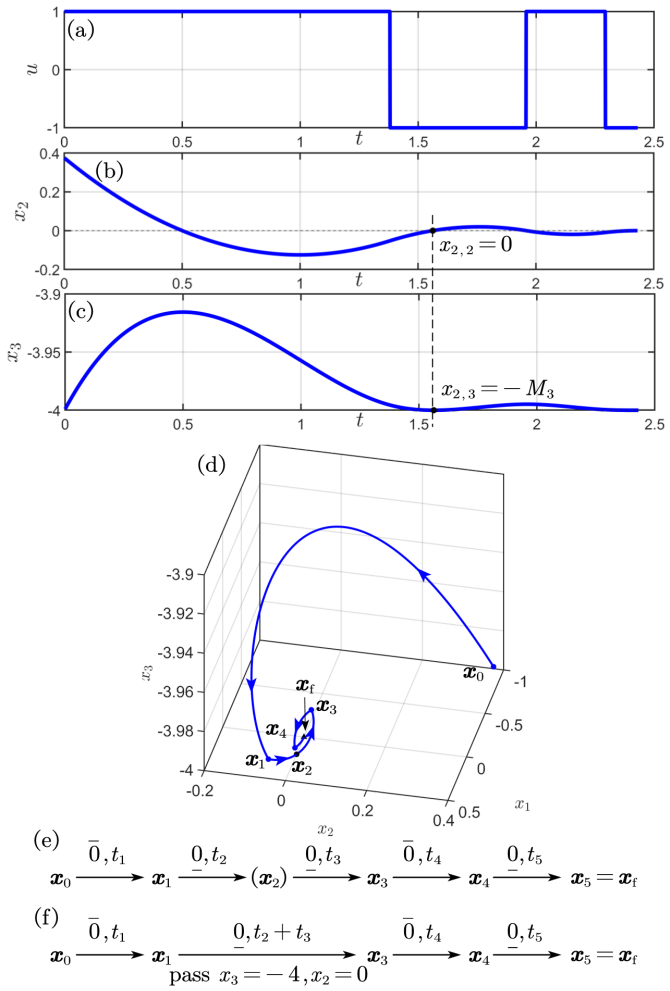

Fig. 6. Time-optimal trajectory with a tangent marker. $\mathcal{P}=\mathcal{P}(\boldsymbol{x}_0,\boldsymbol{x}_f;\boldsymbol{M})$, where $\boldsymbol{M}=(1,1,1.5,4)$. An augmented switching law for $\mathcal{P}$ is $S'=\bar{0}\underline{0}(\underline{3},2)\,\underline{0}\bar{0}\underline{0}\in\mathcal{AS}(\mathcal{P})$, where the tangent marker $(\underline{3},2)$ means $x_{2,3}=-4, x_{2,2}=0$, and $x_{2,1}>0$. (a), (b) and (c) are the jerk, velocity, and position plots, respectively. (d) is the trajectories of system states $\boldsymbol{x}$. (e) and (f) are the flow charts for $S'\in\mathcal{AS}(\mathcal{P})$ and $S=\mathcal{S}(\mathcal{P})\,\bar{0}\underline{0}\bar{0}\underline{0}$.

then the full definite conditions are provided by (19), (20), and (21). However, $S=\bar{0}\underline{0}\bar{0}$ is underdefined, while $S=\bar{0}$ is overdefined; hence, the optimal control can be solved directly from neither $S=\bar{0}\underline{0}\bar{0}$ nor $S=\bar{0}$ by (19), (20), and (21). The augmented switching law should be proposed to solve the problem.

Definition 7. Given a problem $\mathcal{P}$, an **augmented switching law** w.r.t. $\mathcal{P}$, denoted as $S\in\mathcal{AS}(\mathcal{P})$, is the switching law of $\mathcal{P}$ attached full definite conditions.

Definite conditions attached to an augmented switching law S should guarantee that $\dim S=n$ for an n-th order problem. In the above example where $n=2$, $\dim\bar{0}\underline{0}=2$, $\dim\bar{0}\underline{0}\bar{0}=3>2$, and $\dim\bar{0}<2$. Therefore, $\bar{0}\underline{0}$ provides full definite conditions and is an augmented switching law, while $\bar{0}\underline{0}\bar{0}$ and $\bar{0}$ are not. As a trick, the switching law $\bar{0}$ can be represented by an augmented switching law $\underline{0}\bar{0}$ or $\bar{0}\underline{0}$, where the motion time of $\underline{0}$ is 0. This example also shows that the augmented switching law of a problem can be not unique.

However, the above trick of adding zeros is not enough to provide all augmented switching laws. According to the discussion on Case 2 in Section III-A2, the tangent marker is necessary to be defined as a kind of definite condition and precisely exists in the time-optimal problem (1).

Definition 8. For a time-optimal trajectory, assume $|x_k|$ touches M_k at t_1 with a degree $h=k$ or an even degree $h<k$, as described in Theorem 1-6. Then, the **tangent marker** is denoted as (s,h), where $|s|=k$ and $\operatorname{sgn}(s)=\operatorname{sgn}(x_k(t_1))$.

Theorem 4. *$S=S_1(s,h)S_2$ where $S_i=s_1^{(i)}s_2^{(i)}\dots s_{N_i}^{(i)}$ are augmented switching laws, $i=1,2$, then,*

1) $\left|s_{N_1}^{(1)}\right|=\left|s_1^{(2)}\right|=0$.
2) *(s,h) contributes $-h<0$ dimension.*

Proof. According to Section III-A2, $\left|s_{N_1}^{(1)}\right|=\left|s_1^{(2)}\right|=0$, and (s,h) does not provide extra motion time. Assume the state vector at (s,h) is $\boldsymbol{x}_1$. Then, (s,h) contributes h extra constraints, i.e., $x_{1,|s|}=\operatorname{sgn}(s)M_{|s|}$, and $x_{1,|s|-k}=0$, $k=1,2,\dots,h-1$. Hence, (s,h) contributes $-h$ dimension. □

Fig. 6 shows an example of the tangent marker. From Fig. 6(a), it is observed that $\mathcal{S}(\mathcal{P})=\bar{0}\underline{0}\bar{0}\underline{0}$. Therefore, $\dim\mathcal{S}(\mathcal{P})=4>3$. Hence, the problem $\mathcal{P}$ is not determined by $\mathcal{S}(\mathcal{P})$. Opportunely, $S'=\bar{0}\underline{0}(\underline{3},2)\,\underline{0}\bar{0}\underline{0}\in\mathcal{AS}(\mathcal{P})$, where the tangent marker $(\underline{3},2)$ induced 2 constraints, i.e., $x_{2,3}=-M_2$ and $x_{2,2}=0$. Therefore, $\dim S'=5-2=3$, and $\mathcal{P}$ is determined by S'. As shown in Fig. 6(f), $\underline{0}(\underline{3},2)\,\underline{0}$ with time t_2,t_3 performs the same as $\underline{0}$ with time t_2+t_3 on the surface, and $(\underline{3},2)$ means the system state vector passes $x_3=-4$, $x_2=0$ during the stage $\underline{0}$.

The physical meaning of the tangent marker $(\underline{3},2)$ is clear. Without consideration of the constraint $x_3\geq-M_3$, the switching law should be $\underline{0}\bar{0}\underline{0}$, where $x_3<-M_3$ occurs. To guarantee $x_3\geq-M_3$, an accelerating stage $\bar{0}$ is introduced first, then $\underline{0}\bar{0}\underline{0}$ is applied for minimum motion time. The tangent marker $(\underline{3},2)$ shows that the first stage $\bar{0}$ lasts as short as possible. In other words, once the constraint $x_3\geq-M_3$ holds in the future, an optimal switching law $\underline{0}\bar{0}\underline{0}$ is applied. Therefore, the constraint $x_3\geq-M_3$ is active, and $(\underline{3},2)$ reflects some conditions for extremum.

Considering the full discussion in Section III-A, a conjecture is proposed that system behaviors and tangent markers can provide full definite conditions for time-optimal trajectories.

Conjecture 1. *$\forall S$ is an augmented switching law of the time-optimal problem* (1) *where chattering phenomena do not occur, S consists of system behaviors in Definition 1 and tangent markers in Definition 8.*

Obviously, if Conjecture 1 can be proven constructively, then there is a prospect of the time-optimal problem for high-order chain-of-integrator systems which is an open problem in the optimal control theory.

IV. Manifold-Intercept Method

Section III studies the properties of time-optimal control and builds a novel notation system of the time-optimal problem for chain-of-integrators. However, it is a daunting task to solve the

optimal control for arbitrary given problems $\mathcal{P}(\boldsymbol{x}_0, \boldsymbol{x}_\mathrm{f}; \boldsymbol{M})$, especially when a chattering phenomenon occurs. Based on conclusions of optimal control reasoned in Section III, this section proposes a trajectory planning method for high-order chain-of-integrators systems, named the manifold-intercept method (MIM).

It should be pointed out that MIM is an efficient and quasi-optimal method. As is pointed out in our related work [42], chattering phenomena exist in 4th order or higher-order problems, which impedes the computation of optimal control. Section V will indicate that MIM is near-optimal for 4th or higher-order problems, and is able to avoid chattering. Furthermore, for 3rd or lower-order problems, MIM achieves time-optimality. In this section, the switching law and the optimal-trajectory manifold are corresponding to those induced by MIM. Propositions in Section III except for Conjecture 1 still hold true, while theorems in this section might not be true for time-optimal control unless emphasized.

A. Manifold-Intercept Method

The key idea of MIM is to follow a greedy and conservative principle. When the current state vector is "higher" (or "lower") than the lower-order optimal-trajectory manifold of the terminal state vector, the control greedily chooses the minimum (or maximum) value to drive the system to enter the constant velocity phase of minimum (or maximum) velocity, i.e., $\underline{n-1}$ (or $\overline{n-1}$) as quick as possible, conservatively considering state constraints. Once the states enter the lower order optimal-trajectory manifold, the states move along lower order trajectories to reach the terminal states, where the Bellman's principle of optimality [47] is applied.

Definition 9. The **proper-position function** is defined as $p^*: \operatorname{dom} p^* \to \mathbb{R}$, $(\boldsymbol{x}_0, \boldsymbol{x}_\mathrm{f}; \boldsymbol{M}) \mapsto \hat{x}_n$, where

$$\operatorname{dom} p^* = \{(\boldsymbol{x}_0; \boldsymbol{x}_\mathrm{f}, \boldsymbol{M}) : \mathcal{P}(\boldsymbol{x}_0, \boldsymbol{x}_\mathrm{f}; \boldsymbol{M}) \text{ is feasible}, \boldsymbol{x}_0, \boldsymbol{x}_\mathrm{f} \in \mathbb{R}^n, \boldsymbol{M} \in \mathbb{R}_{++} \times \overline{\mathbb{R}}_{++}^n\}, \quad (24)$$

s.t. $\hat{\boldsymbol{x}}_0 \triangleq (x_{0,1}, x_{0,2}, \ldots, x_{0,n-1}, \hat{x}_n) \in \mathcal{F}_{n-1}(\boldsymbol{x}_\mathrm{f}, \boldsymbol{M})$.

Definition 10. For a feasible problem $\mathcal{P}(\boldsymbol{x}_0, \boldsymbol{x}_\mathrm{f}; \boldsymbol{M})$ of n-th order, $\boldsymbol{x}_0$ is called **higher** (or **lower**) than $\mathcal{F}_{n-1}(\boldsymbol{x}_\mathrm{f}, \boldsymbol{M})$, if $x_{0,n} >$ (or $<$) $p^*(\boldsymbol{x}_0; \boldsymbol{x}_\mathrm{f}, \boldsymbol{M})$. If $x_{0,n} = p^*(\boldsymbol{x}_0; \boldsymbol{x}_\mathrm{f}, \boldsymbol{M})$, then $\boldsymbol{x}_0$ is called to **have a proper position**.

The proper-position function is well-defined according to Proposition 4. In Definition 9, $\hat{\boldsymbol{x}}_0$ can be regarded as the projection of $\boldsymbol{x}_0$ along the x_n-axis onto $\mathcal{F}_{n-1}(\boldsymbol{x}_\mathrm{f}, \boldsymbol{M})$. In Definition 10, the relationship between $\boldsymbol{x}_0$ and $\mathcal{F}_{n-1}(\boldsymbol{x}_\mathrm{f}, \boldsymbol{M})$ is represented by the positional relationship between $\boldsymbol{x}_0$ and its projection, i.e., $\hat{\boldsymbol{x}}_0$.

A 3rd order example is shown in Fig. 7. $\boldsymbol{x}_0^{(1)}$ is higher than $\mathcal{F}_2(\boldsymbol{x}_\mathrm{f}, \boldsymbol{M})$, while $\boldsymbol{x}_0^{(2)}$, $\boldsymbol{x}_0^{(3)}$, and $\boldsymbol{x}_0^{(4)}$ are lower than $\mathcal{F}_2(\boldsymbol{x}_\mathrm{f}, \boldsymbol{M})$. $\forall i$, $\hat{\boldsymbol{x}}_0^{(i)} \in \mathcal{F}_2(\boldsymbol{x}_\mathrm{f}, \boldsymbol{M})$ has a proper position.

Now MIM is introduced by mathematical induction.

For the base case, i.e., $n = 1$, the optimal control has a trivial analytic expression, i.e.,

$$u^*(t) = M_0 \operatorname{sgn}(x_\mathrm{f} - x_0), \forall 0 \le t \le t_\mathrm{f} = \frac{|x_\mathrm{f} - x_0|}{M_0}. \quad (25)$$

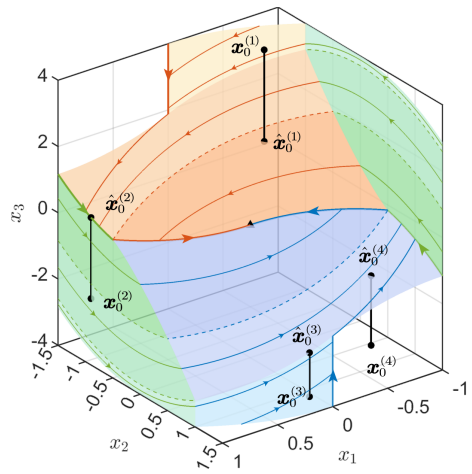

Fig. 7. Some examples of proper positions. The parameters and optimal-trajectory manifold is the same as Fig. 5(b). $\forall i = 1, 2, 3, 4$, $\hat{\boldsymbol{x}}_0^{(i)}$ has a proper position and the same x_1, x_2, x_3 as those of $\boldsymbol{x}_0^{(i)}$.

Assume that $\forall 1 \le k < n$, MIM can plan the k-th order trajectories. In the case where $n \ge 2$ and $M_n = \infty$, $\hat{x}_n = p^*(\boldsymbol{x}_0; \boldsymbol{x}_\mathrm{f}, \boldsymbol{M})$ can be calculated by solving $\mathcal{P}\left(\boldsymbol{x}_0^{1:(n-1)}, \boldsymbol{x}_\mathrm{f}{}^{1:(n-1)}; \boldsymbol{M}^{0:(n-1)}\right)$. One can judge whether $\boldsymbol{x}_0$ is higher or lower than $\mathcal{F}_{n-1}(\boldsymbol{x}_\mathrm{f}, \boldsymbol{M})$ by Definition 9.

1) If $\boldsymbol{x}_0$ has a proper position, according to (16), $\mathcal{P} \triangleq \mathcal{P}(\boldsymbol{x}_0, \boldsymbol{x}_\mathrm{f}; \boldsymbol{M})$ has the same solution as the $(n-1)$-th order problem $\mathcal{P}\left(\boldsymbol{x}_0^{1:(n-1)}, \boldsymbol{x}_\mathrm{f}{}^{1:(n-1)}; \boldsymbol{M}^{0:(n-1)}\right)$.
2) If x_0 is higher than $\mathcal{F}_{n-1}(\boldsymbol{x}_\mathrm{f}, \boldsymbol{M})$, the system tends to achieve the minimum uniform speed $-M_{n-1}$, and keeps the velocity as $-M_{n-1}$ until entering $\mathcal{F}_{n-1}(\boldsymbol{x}_\mathrm{f}, \boldsymbol{M})$.
   a) Firstly, the system state vector moves along the MIM-trajectory of the $(n-1)$-th order problem $\mathcal{P}_1 = \mathcal{P}\left(\boldsymbol{x}_0^{1:(n-1)}, -M_{n-1}\boldsymbol{e}_{n-1}; \boldsymbol{M}^{0:(n-1)}\right)$, i.e., $\boldsymbol{x}(t) = \boldsymbol{x}^*(t; \mathcal{P}_1)$.
   b) If $\boldsymbol{x}(t_\mathrm{f}^*(\mathcal{P}_1))$ is still higher than $\mathcal{F}_{n-1}(\boldsymbol{x}_\mathrm{f}, \boldsymbol{M})$, denote $\hat{x}_n = p^*(-M_{n-1}\boldsymbol{e}_{n-1}; \boldsymbol{x}_\mathrm{f}, \boldsymbol{M})$. Then, $u(t) \equiv 0$ for $t \in [t_\mathrm{f}^*(\mathcal{P}_1), t_1 + t_\mathrm{f}^*(\mathcal{P}_1)]$, where $t_1 = [x_n(t_\mathrm{f}^*(\mathcal{P}_1)) - \hat{x}_n]/M_{n-1}$. Therefore, $\boldsymbol{x}(t_1) = -M_{n-1}\boldsymbol{e}_{n-1} + \hat{x}_n\boldsymbol{e}_n$ has a proper position. Denote $\mathcal{P}_2 = \mathcal{P}\left(-M_{n-1}\boldsymbol{e}_{n-1}, \boldsymbol{x}_\mathrm{f}{}^{1:(n-1)}; \boldsymbol{M}^{0:(n-1)}\right)$. Let $\boldsymbol{x}$ moves along the MIM-trajectory of $\mathcal{P}_2$, i.e., $\boldsymbol{x}(t_\mathrm{f}^*(\mathcal{P}_1) + t_1 + t) = \boldsymbol{x}^*(t; \mathcal{P}_2), 0 \le t \le t_\mathrm{f}^*(\mathcal{P}_2)$. Finally, $\boldsymbol{x}(t_\mathrm{f}^*(\mathcal{P}))$ reaches $\boldsymbol{x}_\mathrm{f}$, i.e.,
   $$t_\mathrm{f}^*(\mathcal{P}) = t_\mathrm{f}^*(\mathcal{P}_1) + t_1 + t_\mathrm{f}^*(\mathcal{P}_2). \quad (26)$$
   c) If $\boldsymbol{x}(t_\mathrm{f}^*(\mathcal{P}_1))$ is lower than $\mathcal{F}_{n-1}(\boldsymbol{x}_\mathrm{f}, \boldsymbol{M})$, i.e., $\boldsymbol{x}(t)$ enters $\mathcal{F}_{n-1}(\boldsymbol{x}_\mathrm{f}, \boldsymbol{M})$ at some time $t_2 \in (0, t_\mathrm{f}^*(\mathcal{P}_1))$, then $\boldsymbol{x}$ can move along the MIM-trajectory of the $(n-1)$-th order problem $\mathcal{P}_3 = \mathcal{P}\left(\boldsymbol{x}^{1:(n-1)}(t_2), \boldsymbol{x}_\mathrm{f}{}^{1:(n-1)}; \boldsymbol{M}^{0:(n-1)}\right)$. Finally, $\boldsymbol{x}(t_\mathrm{f}^*(\mathcal{P}))$ reaches $\boldsymbol{x}_\mathrm{f}$, i.e.,
   $$t_\mathrm{f}^*(\mathcal{P}) = t_2 + t_\mathrm{f}^*(\mathcal{P}_3). \quad (27)$$
3) If x_0 is lower than $\mathcal{F}_{n-1}(\boldsymbol{x}_\mathrm{f}, \boldsymbol{M})$, a similar analysis as above applies to this case.

If $M_{n-1} = \infty$ above, then the first terminal state vector in Case 2 is modified as $-M_k \boldsymbol{e}_k$ where $k < n-1$ is the maximum index satisfying $M_k \neq \infty$. Specifically, if $k = 0$, the problem degenerates into a time-optimal problem without state constraints, which can be easily solved by an n-th order polynomial system [14].

An example of Case 2b is $\boldsymbol{x}^{(1)}$ in Fig. 4, where $\boldsymbol{x}^{(1)}$ slides uniformly under a minimum velocity $-M_1$ until $\boldsymbol{x}$ enters $\mathcal{F}_1(\boldsymbol{x}_\mathrm{f}, \boldsymbol{M})$. An example of Case 2c is $\boldsymbol{x}^{(2)}$ in Fig. 4, where $\boldsymbol{x}^{(2)}$ is intercepted by $\mathcal{F}_1(\boldsymbol{x}_\mathrm{f}, \boldsymbol{M})$ before $\boldsymbol{x}^{(2)}$ reaches $x_1 = -M_1$.

The above n-th order process meets the Bang-Singular-Bang control law and can be solved by sequential $(n-1)$-th order problems. Furthermore, the trajectory $\boldsymbol{x}(t) = \boldsymbol{x}^*(t, \mathcal{P})$ meets the constraints $\forall k = 1, 2, \ldots, n$, $|x_k| \leq M_k$. Specifically, $|x_n| \leq M_n = \infty$.

In the case where $n \geq 2$ and $M_n < \infty$, the optimal trajectory $\boldsymbol{x}(t) = \boldsymbol{x}^*(t; \mathcal{P}_\infty)$ is generated based on the above process, where $\mathcal{P}_\infty = \mathcal{P}\left(\boldsymbol{x}_0, \boldsymbol{x}_\mathrm{f}; \boldsymbol{M}^{0:(n-1)}\right)$.

1) If the trajectory $\boldsymbol{x}(t) = \boldsymbol{x}^*(t; \mathcal{P}_\infty)$ meets the constraint $|x_n| \leq M_n$, then the constraint $|x_n| \leq M_n$ is deactivated. Hence, $\boldsymbol{x}(t) = \boldsymbol{x}^*(t; \mathcal{P}_\infty)$ is also the optimal trajectory of $\mathcal{P} = \mathcal{P}(\boldsymbol{x}_0, \boldsymbol{x}_\mathrm{f}; \boldsymbol{M})$.
2) If the trajectory $\boldsymbol{x}(t) = \boldsymbol{x}^*(t; \mathcal{P}_\infty)$ does not meet the constraint, i.e., $|x_n| > M_n$ at some time, then a tangent marker w.r.t. x_n occurs in the optimal problem $\mathcal{P}$. Considering the dimension of the augmented switching law and according to Theorem 1, $\exists h \leq n$, s.t. $\boldsymbol{x}$ reaches a tangent marker (n, h) through an augmented switching law of h dimension in optimal time, i.e., by solving an h-th order problem. Assume the system state vector is $\hat{\boldsymbol{x}}$ when reaching the tangent marker. Then, the system state vector can move from $\hat{\boldsymbol{x}}$ to $\boldsymbol{x}_\mathrm{f}$ in optimal time by solving $\mathcal{P}\left(\hat{\boldsymbol{x}}, \boldsymbol{x}_\mathrm{f}; \boldsymbol{M}^{0:(n-1)}\right)$.

By mathematical induction, $\forall n \in \mathbb{N}^*$, trajectories for high-order chain-of-integrators systems with full state constraints $\boldsymbol{M} \in \mathbb{R}_{++} \times \overline{\mathbb{R}}_{++}^n$ and arbitrary terminal state vector $\boldsymbol{x}_\mathrm{f} \in \mathbb{R}^n$ can be planned by MIM.

B. Virtual System Behavior

The augmented switching law in this section refers to the switching law in MIM with full definite conditions. The virtual system behavior is defined in the case where (27) occurs.

Definition 11. In MIM, assume that an augmented switching law is $S = S_1 s(S_2) S_3 \in \mathcal{AS}(\mathcal{P}(\boldsymbol{x}_0, \boldsymbol{x}_\mathrm{f}; \boldsymbol{M}))$, where s is a system behavior, and $S_i = s_1^{(i)} s_2^{(i)} \ldots s_{N_i}^{(i)}, i = 1, 2, 3$ are parts of augmented switching laws. (S_2) is a **virtual system behavior**, if $\exists \boldsymbol{t}^{(i)} = \left(t_j^{(i)}\right)_{j=1}^{N_i} \geq \boldsymbol{0}$ and $t_1, t_2 \geq 0$, s.t.

1) $\boldsymbol{x}_0$ moves to $\boldsymbol{x}_\mathrm{f}$ successively passing through S_1 by time $\boldsymbol{t}^{(1)}$, s by time t_1, and S_3 by time $\boldsymbol{t}^{(3)}$. In other words, $S_1 s S_3$ with time $\left(\boldsymbol{t}^{(1)}, t_1, \boldsymbol{t}^{(3)}\right)$ is the solution of $\mathcal{P}$.
2) $\boldsymbol{x}_0$ can move successively passing through S_1 by time $\boldsymbol{t}^{(1)}$, s by time t_2, and S_2 by time $\boldsymbol{t}^{(2)}$. In other words, $S_1 s S_2$ with time $\boldsymbol{t}^{(1)}, t_2, \boldsymbol{t}^{(2)}$ is a feasible solution under constraints (20) and (21).

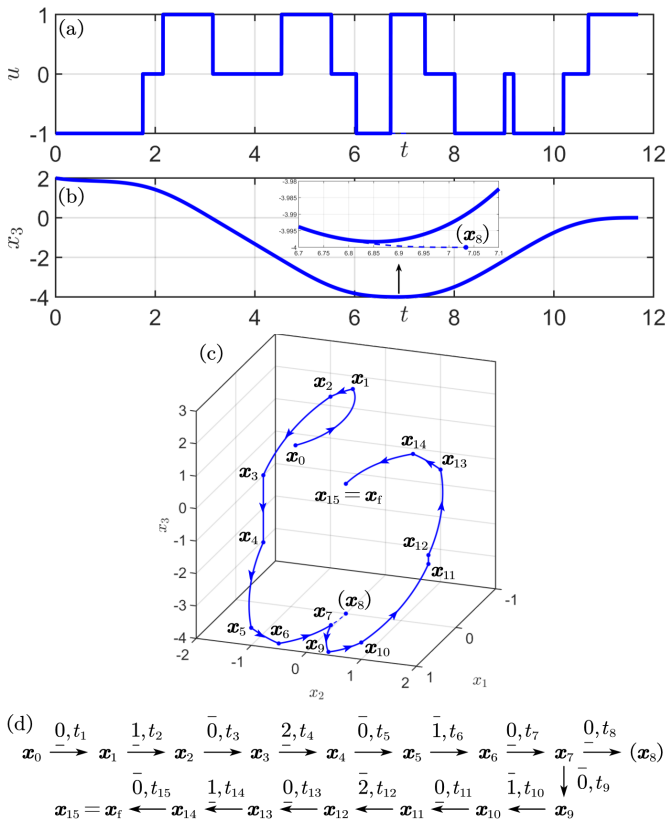

Fig. 8. An example of the virtual system behavior. $\boldsymbol{M} = (1, 1, 1.5, 4, 20)$. $S = \underline{01}\bar{0}\underline{2}\bar{0}\underline{1}0\,(\underline{3})\,\bar{0}\underline{1}0\underline{2}\bar{0}\underline{1}\bar{0} \in \mathcal{AS}(\mathcal{P})$, where $(\underline{3})$ is a virtual system behavior. (a) and (b) are the snap and velocity plots. (c) is the trajectory of $\boldsymbol{x}^{1:3}$. (d) is the flow charts for S.

In Definition 11, S_i is a part of augmented switching laws. In other words, for all i and j, $s_j^{(i)}$ is a system behavior, a tangent marker, or a virtual system behavior. An example is shown in Fig. 8, where $\mathcal{S}(\mathcal{P}) = \underline{01}\bar{0}\underline{2}\bar{0}\underline{1}0\bar{0}\underline{1}0\underline{2}\bar{0}\underline{1}\bar{0}$ in MIM; hence, $\dim \mathcal{S}(\mathcal{P}) = 6 > 4$. $S = \underline{01}\bar{0}\underline{2}\bar{0}\underline{1}0\,(\underline{3})\,\bar{0}\underline{1}0\underline{2}\bar{0}\underline{1}\bar{0} \in \mathcal{AS}(\mathcal{P})$; hence, $\dim S = 4$. As shown in Fig. 8(d), $\boldsymbol{x}_{i-1}$ moves to $\boldsymbol{x}_i$ under the corresponding system state vector for time t_i, $i \neq 8, 9$, while $\boldsymbol{x}_7$ moves to $\boldsymbol{x}_9$ under $\bar{0}$ for time t_9. The ability of $\boldsymbol{x}_7$ to move to $\boldsymbol{x}_8$ under $\bar{0}$ for a time period t_9 provides definite condition for $\mathcal{P}_2$, where $\boldsymbol{x}_8$ is determined by the virtual system behavior $(\underline{3})$, i.e., $x_{8,1} = x_{8,2} = 0$, and $x_{8,3} = -M_3 = -4$. $\boldsymbol{x}$ is intercepted by $\mathcal{F}_3(\boldsymbol{x}_\mathrm{f}, \boldsymbol{M})$ at $\boldsymbol{x}_7$.

Theorem 5. *In MIM, apply the notations from Definition 11.*

1) *The dimension of S can be calculated like* (18)*, i.e., (S_2) contributes $\sum_{i=1}^{N_2}\left(1 - \left|s_i^{(2)}\right|\right) < 0$ dimension to S.*
2) $\left|s_1^{(3)}\right| = 0$*, and* $\operatorname{sgn}(s) = -\operatorname{sgn}\left(s_1^{(3)}\right)$.
3) $\left|s_{N_2}^{(2)}\right| \neq 0$*, and* $\forall k < N_2$, $\left|s_{N_2}^{(2)}\right| > \left|s_k^{(2)}\right|$*. Furthermore,* $\operatorname{sgn}\left(s_{N_2}^{(2)}\right) = -\operatorname{sgn}\left(s_1^{(3)}\right)$.
4) *Except the tangent marker, S_2 has an even number of even numbers, and* (23) *holds.*
5) *If $\exists N_2' < N_2$, s.t. $\dim S_{2,(N_2'+1):N_2} = 0$, then (S_2) is equivalent to $\left(S_{2,1:N_2'}\right)$, i.e., S is equivalent to $S_1 s\left(S_{2,1:N_2'}\right) S_3$.*

Proof. Theorem 5-1 holds by the same analysis as that of Theorem 2. Theorem 5-5 holds evidently.

Denote $\mathcal{P}=\mathcal{P}(\boldsymbol{x}_0,\boldsymbol{x}_\mathrm{f};\boldsymbol{M})$. According to Section IV-A, the virtual system behavior (S_2) occurs when the optimal trajectory represented by S_1sS_2 is intercepted by a low-dimensional optimal-trajectory manifold $\mathcal{F}$, and $\boldsymbol{x}$ moves in $\mathcal{F}$ along an optimal trajectory represented by S_3 after that. By induction, we only need to prove Theorem 5 in the case where the terminal state vector of S_1sS_2 has a maximum velocity, i.e., $\left|s_{N_2}^{(2)}\right|=n-1$ for an n-th order problem.

According to the discussion above, $S_3\in\mathcal{AF}_{n-1}$; hence, $\left|s_1^{(3)}\right|=0$. Note that S_1sS_3 induces $\mathcal{S}(\mathcal{P})$ by removing all brackets, and s as well as $s_1^{(3)}$ are system behaviors. According to Theorem 3, $\mathrm{sgn}(s)=-\mathrm{sgn}\left(s_1^{(3)}\right)$. Theorem 5-2 holds.

Note that $S_1sS_2^{1:(N_2-1)}$ is an augmented switching law with the terminal states $\pm M_{n-1}\boldsymbol{e}_{n-1}$. Therefore, $\left|s_{N_2}^{(2)}\right|=n-1\neq 0$, and $\left|s_{N_2}^{(2)}\right|>\left|s_k^{(2)}\right|,\forall k<N_2$. Furthermore, $\left|s_1^{(1)}\right|=\left|s_{N_3}^{(3)}\right|=0$ and $\mathrm{sgn}\left(s_{N_3}^{(3)}\right)=(-1)^{n-1}\mathrm{sgn}\left(s_1^{(1)}\right)$. Note that $S_3\in\mathcal{AF}_{n-1}$; hence, $\mathrm{sgn}\left(s_{N_3}^{(3)}\right)=(-1)^{n-2}\mathrm{sgn}\left(s_1^{(3)}\right)$. Assume $\boldsymbol{x}_0$ is higher than $\mathcal{F}_{n-1}(\boldsymbol{x}_\mathrm{f},\boldsymbol{M})$. Then, $\mathrm{sgn}\left(s_{N_2}^{(2)}\right)=\mathrm{sgn}\left(s_1^{(1)}\right)=-1$; hence, $\mathrm{sgn}\left(s_{N_2}^{(2)}\right)=-\mathrm{sgn}\left(s_{N_3}^{(3)}\right)$. If $\boldsymbol{x}_0$ is lower than $\mathcal{F}_{n-1}(\boldsymbol{x}_\mathrm{f},\boldsymbol{M})$, then $\mathrm{sgn}\left(s_{N_2}^{(2)}\right)=-\mathrm{sgn}\left(s_{N_3}^{(3)}\right)=1$. Therefore, Theorem 5-3 holds.

According to the discussion above, (23) holds for S_1sS_2, S_1sS_3, and $s_{N_2}^{(2)}S_3$. In other words, the sign of $S_1s(S_2)S_3$ is the same as $S_1sS_2S_3$ and satisfies (23). Note that $\mathrm{sgn}(s)=-\mathrm{sgn}\left(s_1^{(3)}\right)=\mathrm{sgn}\left(s_{N_2}^{(2)}\right)$; hence, S_2 has an even number of even numbers. Therefore, Theorem 5-4 holds. □

As an example for Theorem 5-5, $\underline{01\bar{0}2}\left(\overline{01}\underline{03}\right)\overline{01}\underline{0\bar{2}01\bar{0}}$ is equivalent to $\underline{01\bar{0}2\overline{01}0\bar{2}01\bar{0}}$. The tangent marker also exhibits certain properties in MIM.

Theorem 6. *Apply the notations from Theorem 4. In MIM,*

1) $\mathrm{sgn}\left(s_{N_1}^{(1)}\right)=\mathrm{sgn}\left(s_1^{(2)}\right)=\mathrm{sgn}(s)$.
2) $h<|s|$. *Moreover, h is even.*

Proof. Similar to the proof of Theorem 5, we only need to prove the case where $|s|=n$ for an n-th problem. Assume $\boldsymbol{x}_0$ is higher than $\mathcal{F}_{n-1}(\boldsymbol{x}_\mathrm{f},\boldsymbol{M})$ and the tangent marker occurs. According to Theorem 6, $\left|s_{N_1}^{(1)}\right|=\left|s_1^{(2)}\right|=0$. According to Section IV-A, $\mathrm{sgn}(s_1)=(-1)^{d-2}\mathrm{sgn}\left(s_1^{(1)}\right)=-1$, and $\mathrm{sgn}(s)=-1$. When $\boldsymbol{x}$ reaches (s,d) as $\tilde{\boldsymbol{x}}$, $\tilde{\boldsymbol{x}}$ is still higher than $\mathcal{F}_{n-1}(\boldsymbol{x}_\mathrm{f},\boldsymbol{M})$, while s_2S_2 is the augmented switching law from $\tilde{\boldsymbol{x}}$ to $\boldsymbol{x}_\mathrm{f}$. Therefore, $|s_2|=0$, $\mathrm{sgn}(s_1)=-1$. Applying a similar analysis to the case where $\boldsymbol{x}_0$ is lower than $\mathcal{F}_{n-1}(\boldsymbol{x}_\mathrm{f},\boldsymbol{M})$, Theorem 6-1 holds.

Assume $h=|s|$ and the system state vector reaches (s,h) at t. Then, u is continuous at t and $u(t)=\mathrm{sgn}(s)M_0$ by Theorem 6-1. However, according to Section III-A2, $\mathrm{sgn}(u(t))=-\mathrm{sgn}(s)$ since $\left|x_{|s|}\right|\leq M_{|s|}$, which causes contradiction. Therefore, $h<|s|$; hence, h is even. □

Theorems 5 and 6 indicate that signs of elements of an augmented switching law of length N are determined by the sign of the last element, which also reduces the possible signs of all elements from 2^N to 2. Then, augmented switching laws can be enumerated fully, as reasoned in Section IV-C.

C. Full Enumeration of Augmented Switching Laws in MIM

Definition 12. In MIM, assume $\mathcal{F}_k(\boldsymbol{x}_\mathrm{f},\boldsymbol{M})\neq\varnothing$ in (16). The **augmented-switching-law representation** of $\mathcal{F}_k(\boldsymbol{x}_\mathrm{f},\boldsymbol{M})$ is

$$\mathcal{AF}_k(\boldsymbol{x}_\mathrm{f},\boldsymbol{M})=\bigcup\{S\in\mathcal{AS}(\mathcal{P}(\boldsymbol{x}_0,\boldsymbol{x}_\mathrm{f};\boldsymbol{M})):\boldsymbol{x}_0\in\mathcal{F}_k(\boldsymbol{x}_\mathrm{f},\boldsymbol{M}),\dim S=k\}. \tag{28}$$

$\forall\boldsymbol{x}_0\in\mathcal{F}_k(\boldsymbol{x}_\mathrm{f},\boldsymbol{M}),\mathcal{P}=\mathcal{P}(\boldsymbol{x}_0,\boldsymbol{x}_\mathrm{f};\boldsymbol{M}),S\in\mathcal{AS}(\mathcal{P})$, if $\dim S=k'<k$, $(k-k')$ zero can be added before S to increase the dimension to k. For example, if $S=\bar{0}\underline{0}$ in Fig. 5(b), the switching law can be seen as $\underline{0\bar{0}0}$, and the motion time solved for the first $\underline{0}$ is 0. If some augmented switching laws do not end with 0, then some zeros can also be added after the augmented switching law with motion time 0.

Definition 13. In MIM,

$$\mathcal{AF}_n\triangleq\bigcup_{\substack{\boldsymbol{x}_\mathrm{f}\in\mathbb{R}^n\\ \boldsymbol{M}\in\mathbb{R}_{++}\times\overline{\mathbb{R}}_{++}^n}}\mathcal{AF}_n(\boldsymbol{x}_\mathrm{f},\boldsymbol{M}) \tag{29}$$

is called the **n-th order set of augmented switching laws**.

By Section IV-A, $\mathcal{AF}_n$ can be constructed as follows:

Theorem 7. *In MIM, $\mathcal{AF}_1=\{0\}$. $\forall n\geq 1,\mathcal{AF}_{n+1}\supset F_{n,1}\cup F_{n,2}\cup F_{n,3}$, where*

$$F_{n,1}=\{S_1sS_2:S_1,S_2\in\mathcal{AF}_n,|s|=n\}, \tag{30}$$

$$F_{n,2}=\{S_1(S_2s)S_3:S_1S_2,S_3\in\mathcal{AF}_n,|s|=n,\ S_2s\ \textit{satisfies Theorem 5-4}\}, \tag{31}$$

$$F_{n,3}=\{S_1(s,d)S_2:S_1\in\mathcal{AF}_d,S_2\in F_{n,1}\cup F_{n,2},\ |s|=n+1,d<|s|\ \textit{is even}\}. \tag{32}$$

The signs of system behaviors, tangent markers, and virtual system behaviors satisfy Theorems 3, 4, 5, and 6.

Proof. According to Theorems 5, 6, and discussion in Section IV-A, Theorem 7 holds evidently. □

For example, $\mathcal{AF}_2$={00, 010}. $\mathcal{AF}_3$={000, 0010, 0100, 01010, 00200, 002010, 010200, 0102010, 00(3,2)000, 00(3,2)0010, 00(3,2)0100, 00(3,2)01010, 00(3,2)00200, 00(3,2)002010, 00(3,2)010200, 00(3,2)0102010, 010(3,2)000, 010(3,2)0010, 010(3,2)0100, 010(3,2)01010, 010(3,2)00200, 010(3,2)002010, 010(3,2)010200, 010(3,2)0102010}. $\mathcal{AF}_4$= {0000, 010(4,2)0102010(3)0102010, ...}. $\mathcal{AF}_n$ for $n\geq 4$ can be obtained by Theorem 7. Moreover, previous works on time-optimal jerk-limited trajectories like [11], [18], [19] are all devoted to studying the first 8 switching law through model-based analysis, failing to completely enumerate $\mathcal{AF}_3$.

All augmented switching laws for any trajectory planning problem for high-order chain-of-integrators systems have been fully enumerated so far. In other words, the suboptimal solution of problem (1) with arbitrary initial states, terminal states, and full state constraints can be solved even by enumeration.

D. Calculation of Motion Time and Feasibility Verification

According to Definition 12 and 13, $\forall S \in \mathcal{AF}_n$, $\dim S = n$. Therefore, the motion time can be determined by a given initial state vector $\boldsymbol{x}_0$ and an augmented switching law S. Denote $\boldsymbol{f} : \mathbb{R}^n \times \mathbb{R} \times \mathbb{R} \to \mathbb{R}^n$ whose k-th component is

$$f_k(\boldsymbol{x}, u, t) = \frac{1}{k!} u t^k + \sum_{i=1}^{k} \frac{1}{i!} x_{k-i} t^i. \tag{33}$$

$\boldsymbol{y} = \boldsymbol{f}(\boldsymbol{x}, u, t)$ means system state vector moves from $\boldsymbol{x}$ to $\boldsymbol{y}$ under a constant control u over a period of time t. Next, describe equations induced by a given $S = s_1 s_2 \dots s_N \in \mathcal{AF}_n$. Assume the system state vector reaches $\boldsymbol{x}_{m-1}$ before s_m. The control and time in stages of s_m are u_m and t_m, respectively. u_m and $\operatorname{sgn}(s_m)$ can be calculated by Theorem 3 and Theorem 5.

If s_m and s_{m+1} are system behaviors, or if s_m and s_{m+1} are the virtual system behaviors, or if $m = N$, then

$$\begin{cases} \boldsymbol{x}_m = \boldsymbol{f}(\boldsymbol{x}_{m-1}, u_m, t_m), \\ x_{m,|s_m|} = \operatorname{sgn}(s_m) M_{|s_m|}, \text{ if } |s_m| \neq 0, \\ x_{m,k} = 0, \text{ if } |s_m| \neq 0, k < |s_m|. \end{cases} \tag{34}$$

For $s_l (s_{l+1} \dots s_{r-1}) s_r$, s_l and s_r are system behaviors, while $(s_{l+1} \dots s_{r-1})$ is a virtual system behavior. According to Theorem 5-2, $s_r = 0$. Then,

$$\begin{cases} \boldsymbol{x}_l = \boldsymbol{f}(\boldsymbol{x}_{l-1}, u_l, t_l), \\ \boldsymbol{x}_{r-1} = \boldsymbol{f}(\boldsymbol{x}_{l-1}, u_l, t_{r-1}), \\ \boldsymbol{x}_r = \boldsymbol{f}(\boldsymbol{x}_{r-1}, u_r, t_r), \\ x_{l,|s_l|} = \operatorname{sgn}(s_l) M_{|s_l|}, \text{ if } |s_l| \neq 0, \\ x_{l,k} = 0, \text{ if } |s_l| \neq 0, k < |s_l|. \end{cases} \tag{35}$$

For $s_{m-1}(s_m, d_m) s_{m+1}$, $u_{m-1} = u_{m+1}$, and u_m is not defined. Then,

$$\begin{cases} \boldsymbol{x}_m = \boldsymbol{f}(\boldsymbol{x}_{m-2}, u_{m-1}, t_{m-1}), \\ x_{m,|s_m|} = \operatorname{sgn}(s_m) M_{|s_m|}, \\ x_{m,|s_m|-k} = 0, \ k < d_m. \end{cases} \tag{36}$$

Finally, $\boldsymbol{x}_N$ is substituted with $\boldsymbol{x}_{\mathrm{f}}$.

Assume $S \in \mathcal{AF}_n$ has N_0 system behaviors, N_1 virtual system behaviors, and N_2 tangent markers. Then, the number of equations equals the number of variables, i.e., $(N_0 + N_1)(n+1) - n$. N_2 satisfies $\dim S = n$.

Feasibility verification is trivial. On one hand, $\forall m = 1, 2, \dots, N$, $t_m \geq 0$. On the other hand, $\forall m = 1, 2, \dots, N$, $\forall t \in [0, t_m]$, $\forall k = 1, 2, \dots, n$, $|x_{m,k}(t)| \leq M_k$, where $x_{m,k}(t)$ is the system state after entering s_m for a period of time t. The latter feasibility condition can be verified by $x_k(t) = f_k(\boldsymbol{x}_p, u_m, t)$, where $\boldsymbol{x}_p$ is the previous system state vector of s_m according to the discussion above. Furthermore, checking $|x_{m,k}(t)| \leq M_k$ at stationary points is enough [26].

Based on MIM in Section IV-A and enumeration of $\mathcal{AF}_n$ in Section IV-C, a trajectory planning algorithm for high-order chain-of-integrators systems with arbitrary initial states, terminal states, and full state constraints is developed in Algorithm 1. By induction, the input control in MIM switches for finite times, noting that at most one tangent marker w.r.t. n is allowed and $\forall 0 \leq j \leq 3$, $\boldsymbol{x}^{(j)}$ is a lower-order trajectory.

Algorithm 1: Trajectory planning for high-order chain-of-integrators systems by MIM.

Input: $n \in \mathbb{N}^*$, $\boldsymbol{x}_0$, $\boldsymbol{x}_{\mathrm{f}} \in \mathbb{R}^n$, $\boldsymbol{M} \in \mathbb{R}_{++} \times \overline{\mathbb{R}}_{++}^{n}$.
Output: Optimal control $u = u^*(t)$ of problem (1).

if $n = 1$ **then**
  Solve the problem by (25) and **return**.
end if
if $\boldsymbol{x}_0$ is higher than $\mathcal{F}_{n-1}\left(\boldsymbol{x}_{\mathrm{f}}; \boldsymbol{M}^{0:(n-1)}\right)$ **then**
  Obtain $u = \hat{u}^*(t)$ by $\mathcal{P}(-\boldsymbol{x}_0, -\boldsymbol{x}_{\mathrm{f}}, \boldsymbol{M})$.
  return $u^*(t) = -\hat{u}^*(t)$.
end if
if $M_1 = M_2 = \cdots = M_{n-1} = \infty$ **then**
  Obtain $\boldsymbol{x}^*(t)$, $u^*(t)$, t_{f} by solving n tandem (33).
else
  $m \leftarrow \arg\max\{k < n : M_k < \infty\}$.
  Obtain $\boldsymbol{x}^{(1)}(t), t_{\mathrm{f1}}$ by $\mathcal{P}\left(\boldsymbol{x}_0^{1:m}, M_m \boldsymbol{e}_m, \boldsymbol{M}^{0:m}\right)$ and let $x_m \equiv M_m$ for $t > t_{\mathrm{f1}}$.
  Solve t_1 when $\boldsymbol{x}$ enters $\mathcal{F}_{n-1}\left(\boldsymbol{x}_{\mathrm{f}}; \boldsymbol{M}^{0:m}\right)$.
  Obtain $\boldsymbol{x}^{(2)}(t)$ by $\mathcal{P}\left(\boldsymbol{x}^{1:(n-1)}(t_1), \boldsymbol{x}_{\mathrm{f}}^{1:(n-1)}, \boldsymbol{M}^{0:m}\right)$.
  Obtain $\boldsymbol{x}^*(t)$ by connecting $\boldsymbol{x}^{(1)}$, $\boldsymbol{x}^{(2)}$.
end if
if $M_n < \infty$ **and** $\exists t \in (0, t_{\mathrm{f}})$, $|x_n^*(t)| > M_n$ **then**
  for $d \leftarrow 2, 4, \dots, 2\left\lfloor \frac{n-1}{2} \right\rfloor$ **do**
    for $S \in \mathcal{AF}_d$ **do**
      Obtain $\boldsymbol{x} = \boldsymbol{x}^{(0)}(t), t_{\mathrm{f0}}$ by S, where $\boldsymbol{x}$ moves from $\boldsymbol{x}_0$ to (n, d);
      Obtain $\boldsymbol{x} = \boldsymbol{x}^{(3)}(t)$ by $\mathcal{P}(\boldsymbol{x}(t_{\mathrm{f0}}), \boldsymbol{x}_{\mathrm{f}}, \boldsymbol{M})$.
      Update the best feasible trajectory $\boldsymbol{x}^*(t)$ by connecting $\boldsymbol{x}^{(0)}, \boldsymbol{x}^{(3)}$.
    end for
  end for
end if

V. Numerical Results and Discussion

A. Simulation Setup

Baselines. To verify the performance of the proposed MIM method, i.e., Algorithm 1, simulation experiments for trajectories are conducted. The baselines are as follows.

- **Ruckig** [19] in community version: a jerk-limited time-optimal trajectory solver without position constraints.
- **SOCPs** [32]: a time-optimal control method based on solving sequential convex second-order cone problems. The SOCPs method is achieved by Gurobi [48].
- **Yop** [31]: a MATLAB toolbox for numerical optimal control problems based on CasADi [29] by direct methods.

The control period of Ruckig is set as 1 ms. The number of time points is set as 500 and 150 in SOCPs and Yop, respectively. In practice, if the number of time points is set more than 600 and 200 in SOCPs and Yop, respectively, then the computational time will increase significantly.

Metrics. For trajectory planning methods, the computational efficiency, the computational error, and the trajectory quality are significant performance metrics.

- The computational time T_{c}. All experiments are conducted in MATLAB 2021b on a computer with an AMD Ryzen 7 5800H @ 3.20 GHz processor.
- The error of the terminal states E_{s}. For a solved final state vector $\hat{\boldsymbol{x}}_{\mathrm{f}}$, E_{s} is defined in normalization as

$$E_{\mathrm{s}} \triangleq \sqrt{\sum_{k=1}^{n}\left(\frac{x_{\mathrm{f}k}-\hat{x}_{\mathrm{f}k}}{M_k}\right)^2}. \tag{37}$$

- The success rate to obtain a feasible solution R_{s}. A result is determined to be successful if the states along the planned trajectories are feasible and $E_{\mathrm{s}} \leq 0.1$.
- The normalized mean-squared error (MSE) E_{m} between the solved $u = u(t)$ and the Bang-Singular-Bang control law [11] is defined to describe the trajectory quality. According to Proposition 1, the optimal control $u^*(t) \in \{0, M_0, -M_0\}$ almost everywhere. Define

$$E_{\mathrm{m}} \triangleq \sqrt{\frac{4}{M_0^2 t_{\mathrm{f}}}\int_0^{t_{\mathrm{f}}} u(t)^2 \wedge \left(|u(t)| - M_0\right)^2 \,\mathrm{d}t}. \tag{38}$$

  Then, the smaller E_{m} is, the closer $u = u(t)$ is to a Bang-Singular-Bang control law, i.e., the better trajectory quality is. Specifically, $E_{\mathrm{m}} \in [0,1]$. Furthermore, $E_{\mathrm{m}} = 0$ if and only if $\forall t \in [0, t_{\mathrm{f}}]$, $u(t) \in \{0, M_0, -M_0\}$ satisfies the Bang-Singular-Bang control law, while $E_{\mathrm{m}} = 1$ if and only if $\forall t \in [0, t_{\mathrm{f}}]$, $|u(t)| = \frac{1}{2}M_0$.
- The normalized total variation [43] T_{v} of the solved control is defined to describe the stability of the trajectory. For $u\left(\frac{k}{n}t_{\mathrm{f}}\right) = u_k$ with $(n+1)$ waypoints, define

$$T_{\mathrm{v}} \triangleq \frac{1}{2nM_0}\sum_{k=1}^{n}\left|u_k - u_{k-1}\right|. \tag{39}$$

  Then, as T_{v} decreases, the trajectory exhibits increased oscillations, i.e., the stability of the trajectory decreases. Specifically, $T_{\mathrm{v}} \in [0,1]$. Furthermore, $T_{\mathrm{v}} = 0$ if and only if $u_k \equiv \mathrm{const}$, while $T_{\mathrm{v}} = 1$ if and only if $u_k = (-1)^k M_0$ or $u_k = (-1)^{k-1} M_0$.

B. Numerical Results

Several trajectories planned by the proposed MIM and baselines are shown in Fig. 9, and the quantitative results of 100 jerk-limited trajectories and 100 snap-limited trajectories are shown in Fig. 10. Among them, 3rd order trajectories in Fig. 10 contain no tangent markers, since Ruckig in community version is not able to plan trajectories with position constraints. Furthermore, tangent markers occur in 3rd order trajectories only if the initial position and the terminal position are both close to boundaries, which occurs with a low probability.

It is noteworthy that the time-optimal problem (1) with an order $n \geq 3$ is non-convex if it is solved directly in discrete time [49]. Hence, discrete methods like Yop might fail to obtain an optimal trajectory, as shown in Fig. 9(a). Though SOCPs successfully transforms problem (1) into sequential convex problems, SOCPs might fail to obtain a feasible solution during iteration in some cases, as shown in Fig. 9(d). Furthermore, trajectories planned by Yop and SOCPs do not meet constraints (1e), causing failure as well. As shown in Fig. 10(a), Yop and SOCPs has a limited success rate, while Ruckig can plan all 3th order trajectories. Supported by the established theory, the proposed MIM succeeds in planning all randomly selected trajectories in 3rd and 4th order.

As shown in Fig. 10(c) and (d), the proposed MIM outperforms all baselines on computational time and computational accuracy. It can be observed that the proposed MIM achieves a computational time reduction of approximately 2 orders of magnitude compared to SOCPs and Yop, while improving computational accuracy by 90.8% (79.0%), 99.6% (99.0%), and 52.1% compared to SOCPs, Yop, and Ruckig, respectively, for 3rd order (4th order) problems on average. Specifically, MIM is not based on discrete time; hence, its computational efficiency keeps constant no matter what the control period is. On the contrary, as a real-time method, Ruckig requires longer computational time with a higher control frequency, but Ruckig is able to achieve a short computational time than the proposed MIM if its control frequency is set lower than 100 Hz, which is not conducive to precise motion control. Furthermore, the upper bound of the computational accuracy of MIM is determined only by the control frequency.

E_{m} and T_{v} shown in Fig. 10(d) and (e) describe the trajectory quality. E_{m} and T_{v} of MIM and Ruckig are evidently lower than those of SOCPs and Yop. Therefore, the proposed MIM and Ruckig achieve much higher trajectory quality. Compared with SOCPs and Yop, trajectories generated by MIM are strict Bang-Singular-Bang. In addition to necessary switching, the input $u(t)$ of the proposed MIM does not exhibit oscillations like those of SOCPs, as shown in Fig. 9(a) and (c). When the trajectory is short enough like Fig. 9(b), SOCPs has a short step width and can avoid oscillations. Quantitatively, MIM achieves a normalized MSE of control E_{m} that is 80.78% (92.3%), 91.9% (92.2%), and 57.2% lower than that of SOCPs, Yop, and Ruckig, respectively, for 3rd order (4th order) problems on average. Taking oscillations into consideration, MIM achieves a normalized total variation of control T_{v} that is 99.6% (99.5%), 97.1% (99.5%), and 10.1% lower than that of SOCPs, Yop, and Ruckig, respectively, for 3rd order (4th order) problems on average.

C. Discussion

By comparing Algorithm 1 of 3rd order and Ruckig in community version [19] with 1-DOF, it can be examined that the proposed MIM plans the same trajectory with Ruckig for a given 3rd order problem. In conjunction with discussion in Section III, the proposed MIM can plan strictly time-optimal trajectories in 3rd order and lower-order with full state constraints. Furthermore, it can be proved by induction that MIM plans optimal trajectories for n-th order problems when only $|u| \leq M_0$ and $|x_1| \leq M_1$ are active.

For 4th and higher-order problems, MIM plans quasi-optimal trajectories since the virtual system behavior in Definition 11 does not exist in time-optimal trajectories. Some more complex behaviors like chattering can occur in 4th and higher-order problems. Although the proposed MIM does not consider the chattering phenomenon in problem (1), MIM

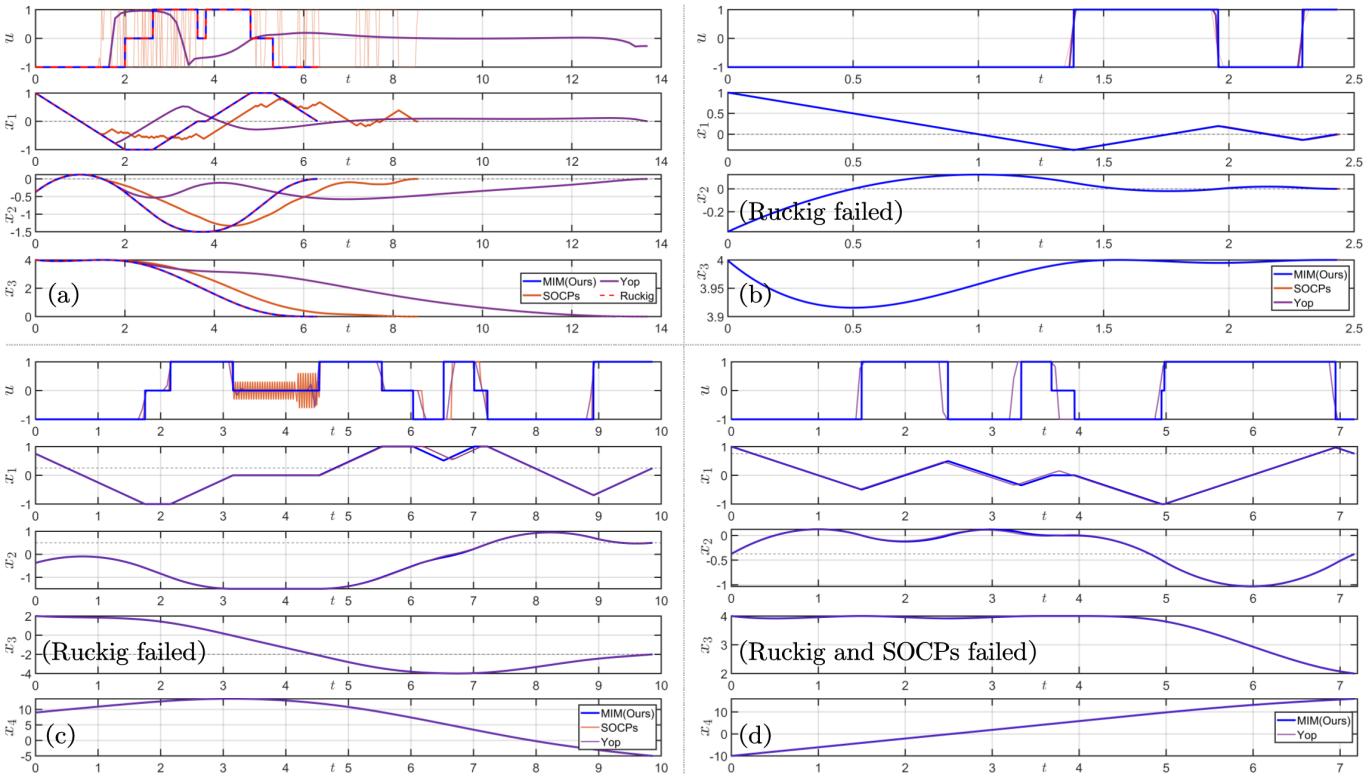

Fig. 9. Some trajectories planned by the proposed and baselines. (a) A jerk-limited trajectory represented by $\underline{01}\bar{0}\underline{2}\overline{01}\underline{0}$. $\boldsymbol{x}_0 = (1, -0.375, 4)$, $\boldsymbol{x}_\mathrm{f} = (0, 0, 0)$, $\boldsymbol{M} = (1, 1, 1.5, 4)$. (b) A jerk-limited trajectory represented by $\underline{0}\bar{0}\,(\overline{3}, 2)\,\bar{0}\underline{0}\bar{0}$. $\boldsymbol{x}_0 = (1, -0.375, 3.999)$, $\boldsymbol{x}_\mathrm{f} = (0, 0, 4)$, $\boldsymbol{M} = (1, 1, 1.5, 4)$. (c) A snap-limited trajectory represented by $\underline{01}\bar{0}\underline{2}\overline{01}\underline{0}(\underline{3})\overline{01}\underline{0}\bar{0}$. $\boldsymbol{x}_0 = (0.75, -0.375, 2, 9)$, $\boldsymbol{x}_\mathrm{f} = (0.25, 0.5, -2, -5)$, $\boldsymbol{M} = (1, 1, 1.5, 4, 20)$. (d) A snap-limited trajectory represented by $\underline{0}\bar{0}(\overline{3}, 2)\bar{0}\underline{0}\bar{0}\underline{3}\overline{01}\underline{0}\bar{0}$. $\boldsymbol{x}_0 = (1, -0.375, 4, -10)$, $\boldsymbol{x}_\mathrm{f} = (0.75, -0.375, 2, 16)$, $\boldsymbol{M} = (1, 1, 1.5, 4, 20)$. The trajectories of MIM and Ruckig almost coincide in (a), while x_3, x_4 of all methods look to coincide.

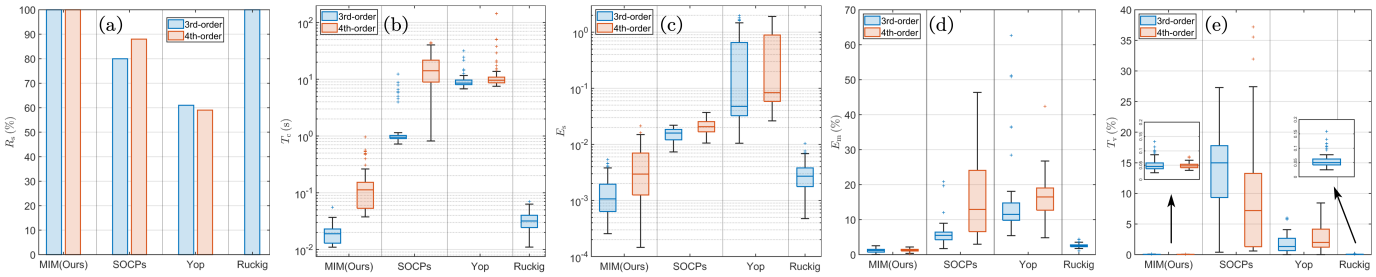

Fig. 10. Quantitative results of 100 3rd order trajectories and 100 4th order trajectories with random initial states and terminal states. (a) Success rate R_s. (b) Computational time T_c. (c) Error of terminal states E_s. (d) Normalized MSE E_m between input and the Bang-Singular-Bang control law. (e) Normalized total variation T_v of the planned control u. Ruckig is only applied in 3rd order trajectories because of disability to plan snap-limited trajectories. y-axes in (b) and (c) are in logarithmic scales.

achieves terminal time close to optimal solution, and avoids infinite times of chattering. For example, a set of typical kinematic parameters for the ultra-precision wafer stage is given in [50], where $M_0 = 64\,000\,\mathrm{m/s^4}$, $M_1 = 790\,\mathrm{m/s^3}$, $M_2 = 10\,\mathrm{m/s^2}$, $M_3 = 0.25\,\mathrm{m/s}$, and $M_4 = 0.02\,\mathrm{m}$. Consider a position-to-position trajectory, i.e., $\boldsymbol{x}_0 = -M_4\boldsymbol{e}_4$ and $\boldsymbol{x}_\mathrm{f} = M_4\boldsymbol{e}_4$. Then, MIM plans a suboptimal trajectory with terminal time $t_{\mathrm{f,MIM}} \approx 0.2100\,\mathrm{s}$. According to [42], the optimal trajectory with chattering achieves terminal time t_f^*, where $t_{\mathrm{f,MIM}} - t_\mathrm{f}^* \approx 29.2\,\mu\mathrm{s}$. So MIM achieves a relative error of 0.014% in terminal time compared to the optimal solution and is able to avoid chattering; note that the control period is usually $200\,\mu\mathrm{s} \gg 29.2\,\mu\mathrm{s}$. Furthermore, if substituting the optimal trajectory in the chattering period by MIM-trajectory, the induced relative error in terminal time is strictly less than 0.12% for any 4th order problems, which is proved in [42]. Therefore, the MIM-trajectory is near-optimal and practical for high-order problems, since chattering does not occur in MIM theoretically according to the process of Algorithm 1.

It is meaningful to strictly solve the time-optimal problem (1) in further study, which would be a landmark achievement in the optimal control theory. To the best of our knowledge, the theoretical framework established in Section III provides unprecedented insights into problem (1), surpassing current literature. Therefore, it is believed that the theoretical framework established in Section III would be a noteworthy mathematical

tool for the final resolution of the time-optimal problem (1).

VI. Conclusion

This paper has set out to theoretically study a classical and challenging problem in the optimal control theory domain, i.e., the time-optimal control problem for high-order chain-of-integrators systems with full state constraints and arbitrary terminal states. To this end, this paper establishes a novel notation system and theoretical framework, providing the switching manifold for high-order problems in the form of switching laws. The framework derives properties of switching laws regarding signs as well as dimension and reasons a definite condition of augmented switching laws. Guided by the developed framework, a trajectory planning method named the manifold-intercept method (MIM) has been proposed, outperforming all baselines by a large gap in computational time, computational accuracy, and trajectory quality. The proposed MIM can achieve time-optimal trajectories for 3rd order or lower-order problems with full state constraints. MIM can also plan near-time-optimal trajectories efficiently and accurately with negligible extra motion time compared to time-optimal trajectories that are in lack of mature algorithms currently, avoiding the chattering phenomenon that impedes numerical computation in practice.

Acknowledgment

The authors would like to thank the anonymous reviewers for their valuable comments and suggestions, to thank Yujie Lin and Hui Ma for their expertise in differential geometry, and to thank Zongying Shi for her experitse in optimal control. This work was supported by the National Key Research and Development Program of China under Grant 2023YFB4302003.

References

[1] W. Wang, C. Hu, K. Zhou, S. He, and L. Zhu, "Local asymmetrical corner trajectory smoothing with bidirectional planning and adjusting algorithm for cnc machining," *Robotics and Computer-Integrated Manufacturing*, vol. 68, p. 102058, 2021.

[2] Z. Wang, R. Zhou, C. Hu, and Y. Zhu, "Real-time iterative compensation based contouring control method for polar coordinate motion systems," *IEEE/ASME Transactions on Mechatronics*, vol. 27, no. 5, pp. 3517–3526, 2022.

[3] Y. Wang, J. Wang, Y. Li, C. Hu, and Y. Zhu, "Learning latent object-centric representations for visual-based robot manipulation," in *2022 International Conference on Advanced Robotics and Mechatronics (ICARM)*. IEEE, 2022, pp. 138–143.

[4] G. Zhao and M. Zhu, "Pareto optimal multirobot motion planning," *IEEE Transactions on Automatic Control*, vol. 66, no. 9, pp. 3984–3999, 2020.

[5] J. Wang, C. Hu, Y. Wang, and Y. Zhu, "Dynamics learning with object-centric interaction networks for robot manipulation," *IEEE Access*, vol. 9, pp. 68 277–68 288, 2021.

[6] C. Ni, M. Zhang, Y. Zhu, C. Hu, S. Ding, and Z. Jia, "Sinusoidal phase-modulating interferometer with ellipse fitting and a correction method," *Applied Optics*, vol. 56, no. 13, pp. 3895–3899, 2017.

[7] M. Li, Y. Zhu, K. Yang, L. Yang, C. Hu, and H. Mu, "Convergence rate oriented iterative feedback tuning with application to an ultraprecision wafer stage," *IEEE Transactions on Industrial Electronics*, vol. 66, no. 3, pp. 1993–2003, 2018.

[8] S. Güler, B. Fidan, S. Dasgupta, B. D. Anderson, and I. Shames, "Adaptive source localization based station keeping of autonomous vehicles," *IEEE Transactions on Automatic Control*, vol. 62, no. 7, pp. 3122–3135, 2016.

[9] Y. Wang, C. Hu, Z. Wang, S. Lin, Z. Zhao, W. Zhao, K. Hu, Z. Huang, Y. Zhu, and Z. Lu, "Optimization-based non-equidistant toolpath planning for robotic additive manufacturing with non-underfill orientation," *Robotics and Computer-Integrated Manufacturing*, vol. 84, p. 102599, 2023.

[10] Y. Wang, C. Hu, Z. Wang, S. Lin, Z. Zhao, and Y. Zhu, "Slice extension for high-quality hybrid additive-subtractive manufacturing," in *IECON 2023-49th Annual Conference of the IEEE Industrial Electronics Society*. IEEE, 2023, pp. 1–6.

[11] S. He, C. Hu, Y. Zhu, and M. Tomizuka, "Time optimal control of triple integrator with input saturation and full state constraints," *Automatica*, vol. 122, p. 109240, 2020.

[12] R. F. Hartl, S. P. Sethi, and R. G. Vickson, "A survey of the maximum principles for optimal control problems with state constraints," *SIAM Review*, vol. 37, no. 2, pp. 181–218, 1995.

[13] E. B. Lee and L. Markus, "Foundations of optimal control theory," Minnesota Univ Minneapolis Center For Control Sciences, Tech. Rep., 1967.

[14] G. Bartolini, S. Pillosu, A. Pisano, E. Usai *et al.*, "Time-optimal stabilization for a third-order integrator: A robust state-feedback implementation," *Lecture Notes in Control and Information Sciences*, pp. 131–144, 2002.

[15] N. Marchand, A. Hably, and A. Chemori, "Global stabilization with low computational cost of the discrete-time chain of integrators by means of bounded controls," *IEEE Transactions on Automatic Control*, vol. 52, no. 5, pp. 948–952, 2007.

[16] Z. Ma and S. Zou, *Optimal control theory: the variational method*. Springer, 2021.

[17] R. Haschke, E. Weitnauer, and H. Ritter, "On-line planning of time-optimal, jerk-limited trajectories," in *2008 IEEE/RSJ International Conference on Intelligent Robots and Systems*. IEEE, 2008, pp. 3248–3253.

[18] T. Kröger, "Opening the door to new sensor-based robot applications–the reflexxes motion libraries," in *2011 IEEE International Conference on Robotics and Automation*. IEEE, 2011, pp. 1–4.

[19] L. Berscheid and T. Kröger, "Jerk-limited real-time trajectory generation with arbitrary target states," in *Robotics: Science and Systems*, 2021.

[20] S. He, C. Hu, S. Lin, Y. Zhu, and M. Tomizuka, "Real-time time-optimal continuous multi-axis trajectory planning using the trajectory index coordination method," *ISA Transactions*, vol. 131, pp. 639–649, 2022.

[21] Y. Gao, K. H. Johansson, and L. Xie, "Computing probabilistic controlled invariant sets," *IEEE Transactions on Automatic Control*, vol. 66, no. 7, pp. 3138–3151, 2020.

[22] U. Walther, T. T. Georgiou, and A. Tannenbaum, "On the computation of switching surfaces in optimal control: A grobner basis approach," *IEEE Transactions on Automatic Control*, vol. 46, no. 4, pp. 534–540, 2001.

[23] E. Khmelnitsky and M. Caramanis, "One-machine n-part-type optimal setup scheduling: analytical characterization of switching surfaces," *IEEE Transactions on Automatic Control*, vol. 43, no. 11, pp. 1584–1588, 1998.

[24] I. M. Mitchell, A. M. Bayen, and C. J. Tomlin, "A time-dependent hamilton-jacobi formulation of reachable sets for continuous dynamic games," *IEEE Transactions on Automatic Control*, vol. 50, no. 7, pp. 947–957, 2005.

[25] F. Tahir and I. M. Jaimoukha, "Low-complexity polytopic invariant sets for linear systems subject to norm-bounded uncertainty," *IEEE Transactions on Automatic Control*, vol. 60, no. 5, pp. 1416–1421, 2014.

[26] L. Doeser, P. Nilsson, A. D. Ames, and R. M. Murray, "Invariant sets for integrators and quadrotor obstacle avoidance," in *2020 American Control Conference (ACC)*. IEEE, 2020, pp. 3814–3821.

[27] M. Yury, "Quasi-time-optimal control of third-order integrators with phase constraints," in *2016 International Conference Stability and Oscillations of Nonlinear Control Systems (Pyatnitskiy's Conference)*. IEEE, 2016, pp. 1–4.

[28] H. Robbins, "Junction phenomena for optimal control with state-variable inequality constraints of third order," *Journal of Optimization Theory and Applications*, vol. 31, pp. 85–99, 1980.

[29] J. A. Andersson, J. Gillis, G. Horn, J. B. Rawlings, and M. Diehl, "Casadi: a software framework for nonlinear optimization and optimal control," *Mathematical Programming Computation*, vol. 11, pp. 1–36, 2019.

[30] Y. Nie, O. Faqir, and E. C. Kerrigan, "Iclocs2: Try this optimal control problem solver before you try the rest," in *2018 UKACC 12th International Conference on Control*. IEEE, 2018, pp. 336–336.

[31] V. Leek, "An optimal control toolbox for matlab based on casadi," 2016.

[32] M. Leomanni, G. Costante, and F. Ferrante, "Time-optimal control of a multidimensional integrator chain with applications," *IEEE Control Systems Letters*, vol. 6, pp. 2371–2376, 2022.

[33] K. Erkorkmaz and Y. Altintas, "High speed cnc system design. part i: jerk limited trajectory generation and quintic spline interpolation," *International Journal of Machine Tools and Manufacture*, vol. 41, no. 9, pp. 1323–1345, 2001.

[34] L. Dai, X. Li, Y. Zhu, M. Zhang, and C. Hu, "The generation mechanism of tracking error during acceleration or deceleration phase in ultraprecision motion systems," *IEEE Transactions on Industrial Electronics*, vol. 66, no. 9, pp. 7109–7119, 2018.

[35] B. Ezair, T. Tassa, and Z. Shiller, "Planning high order trajectories with general initial and final conditions and asymmetric bounds," *The International Journal of Robotics Research*, vol. 33, no. 6, pp. 898–916, 2014.

[36] E. Oland and R. Kristiansen, "Controlling a chain of integrators with constrained actuation using exponential activation functions," in *2019 IEEE 10th International Conference on Mechanical and Aerospace Engineering (ICMAE)*. IEEE, 2019, pp. 258–261.

[37] Y. Wang, "Manifoldinterceptmethod," https://github.com/WangY18/ManifoldInterceptMethod.git, 2024.

[38] L. Berscheid, "Ruckig - motion generation for robots and machines," https://ruckig.com/, 2023.

[39] C. Fox, *An introduction to the calculus of variations*. Courier Corporation, 1987.

[40] H. Maurer, "On optimal control problems with bounded state variables and control appearing linearly," *SIAM Journal on Control and Optimization*, vol. 15, no. 3, pp. 345–362, 1977.

[41] D. H. Jacobson, M. M. Lele, and J. L. Speyer, "New necessary conditions of optimality for control problems with state-variable inequality constraints," *Journal of Mathematical Analysis and Applications*, vol. 35, no. 2, pp. 255–284, 1971.

[42] Y. Wang, C. Hu, Z. Li, Y. Lin, S. Lin, S. He, and Y. Zhu, "Chattering phenomena in time-optimal control for high-order chain-of-integrators systems with full state constraints," *arXiv:2403.17675*, 2024.

[43] E. M. Stein and R. Shakarchi, *Real analysis: Measure theory, integration, and Hilbert spaces*. Princeton University Press, 2009.

[44] D. Trotman, "Stratification theory," *Handbook of Geometry and Topology of Singularities I*, pp. 243–273, 2020.

[45] J. Verbeke and R. Cools, "The newton-raphson method," *International Journal of Mathematical Education in Science and Technology*, vol. 26, no. 2, pp. 177–193, 1995.

[46] Y. Wang, C. Hu, Z. Li, S. Lin, S. He, Z. Wang, and Y. Zhu, "Time-optimal control for high-order chain-of-integrators systems with full state constraints and arbitrary terminal states (extended version)," *arXiv:2311.07039*, 2024.

[47] R. Bellman, "On the theory of dynamic programming," *Proceedings of the national Academy of Sciences*, vol. 38, no. 8, pp. 716–719, 1952.

[48] L. Gurobi Optimization, "Gurobi optimizer reference manual," https://www.gurobi.com, 2023.

[49] F. Debrouwere, W. Van Loock, G. Pipeleers, Q. T. Dinh, M. Diehl, J. De Schutter, and J. Swevers, "Time-optimal path following for robots with convex–concave constraints using sequential convex programming," *IEEE Transactions on Robotics*, vol. 29, no. 6, pp. 1485–1495, 2013.

[50] M. Li, Y. Zhu, K. Yang, and C. Hu, "A data-driven variable-gain control strategy for an ultra-precision wafer stage with accelerated iterative parameter tuning," *IEEE Transactions on Industrial Informatics*, vol. 11, no. 5, pp. 1179–1189, 2015.

Yunan Wang (S'22) received the B.E. degree in mechanical engineering, in 2022, from the Department of Mechanical Engineering, Tsinghua University, Beijing, China. He is currently working toward the Ph.D. degree in mechanical engineering with the Department of Mechanical Engineering, Tsinghua University, Beijing, China.

His research interests include optimal control, trajectory planning, toolpath planning, and precision motion control. He was the recipient of the Best Conference Paper Finalist at the 2022 International Conference on Advanced Robotics and Mechatronics and 2021 Top Grade Scholarship for Undergraduate Students of Tsinghua University.

Chuxiong Hu (S'09-M'11-SM'17) received his B.E. and Ph.D. degrees in Mechatronic Control Engineering from Zhejiang University, Hangzhou, China, in 2005 and 2010, respectively. He is currently a professor (tenured) at Department of Mechanical Engineering, Tsinghua University, Beijing, China. From 2007 to 2008, he was a visiting scholar in mechanical engineering with Purdue University, West Lafayette, USA. In 2018, he was a visiting scholar in mechanical engineering with University of California, Berkeley, CA, USA. His research interests include precision motion control, high-performance multiaxis contouring control, precision mechatronic systems, intelligent learning, adaptive robust control, neural networks, iterative learning control, and robot.

Prof. Hu was the recipient of the Best Student Paper Finalist at the 2011 American Control Conference, the 2012 Best Mechatronics Paper Award from the ASME Dynamic Systems and Control Division, the 2013 National 100 Excellent Doctoral Dissertations Nomination Award of China, the 2016 Best Paper in Automation Award, the 2018 Best Paper in AI Award from the IEEE International Conference on Information and Automation, the 2022 Best Paper in Theory from the IEEE/ASME International Conference on Mechatronic, Embedded Systems and Applications, the 2023 Best Student Paper from the International Conference on Control, Mechatronics and Automation, the 2024 Best Paper Award in Advanced Robotics from the International Conference on Advanced Robotics and Mechatronics, and the 2024 Best Paper Award from the IEEE Conference on Industrial Electronics and Applications. He is now an Associate Editor for the IEEE Transactions on Industrial Informatics and a Technical Editor for the IEEE/ASME Transactions on Mechatronics.

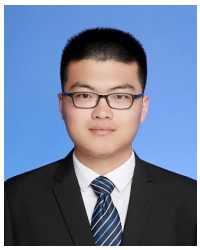

Zeyang Li received the B.E. degree in mechanical engineering from Shanghai Jiao Tong University in 2021, and the M.S. degree in mechanical engineering from Tsinghua University in 2024. He is currently working toward the Ph.D. degree with the Laboratory for Information and Decision Systems, Massachusetts Institute of Technology. His current research interests include reinforcement learning and optimal control.

Shize Lin received the B.E. degree in mechanical engineering, in 2020, from the Department of Mechanical Engineering, Tsinghua University, Beijing, China, where he is currently working toward the Ph.D. degree in mechanical engineering. His research interests include robotics, motion planning and precision motion control.

Suqin He received the B.E. degree in mechanical engineering from Department of Mechanical Engineering, Tsinghua University, Beijing, China, in 2016, and the Ph.D. degree in mechanical engineering from the Department of Mechanical Engineering, Tsinghua University, Beijing, China, in 2023.

His research interests include multi-axis trajectory planning and precision motion control on robotics and CNC machine tools. He was the recipient of the Best Automation Paper from IEEE Internal Conference on Information and Automation in 2016.

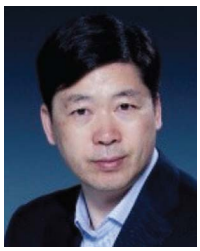

Yu Zhu (Member, IEEE) received the B.E. degree in radio electronics from Beijing Normal University, Beijing, China, in 1983, and the M.S. degree in computer applications and the Ph.D. degree in mechanical design and theory from the China University of Mining and Technology, Beijing, in 1993 and 2001, respectively. He is currently a Professor with the State Key Laboratory of Tribology, Department of Mechanical Engineering, Tsinghua University, China. He has authored or coauthored more than 180 technical papers. He is also the holder of more than 140 warranted invention patents. His research interests include precision measurement and motion control, ultraprecision mechanical design and manufacturing, two-photon microfabrication, and electronics manufacturing technology and equipment.